BUDAPEST UNIVERSITY OF TECHNOLOGY AND ECONOMICS
FACULTY OF MECHANICAL ENGINEERING

FINAL THESIS

Separation of in-plane fracture modes by four equivalent single layers

Author:
Balázs KISS

Supervisors:
Dr. András SZEKRÉNYES

Department of Applied Mechanics

December 9, 2018

Declaration of Authorship

I, Balázs Kiss, the undersigned, hereby declare that the present thesis work has been prepared by myself without any unauthorized help or assistance such that only the specified sources (references, tools, etc.) were used. All parts taken from other sources word by word or after rephrasing but with identical meaning were unambiguously identified with explicit reference to the utilized sources.

I authorize the Faculty of Mechanical Engineering of the Budapest University of Technology and Economics to publish the principal data of the thesis work (author's name, title, abstracts in English and in Hungarian, year of preparation, supervisor's name, etc.) in a searchable, public, electronic and online database and to publish the full text of the thesis work on the internal network of the university (or for authenticated users). I declare that the submitted hard copy of the thesis work and its electronic version are identical. Full text of thesis works classified upon the decision of the Dean will be published after two years.

Budapest, December 9, 2018

. . . . . .

Balázs Kiss

Acknowledgement

I would like to express my great appreciation to my supervisor Dr. András SZEKRÉNYES who supported and inspired me throughout this project. I am thankful for his aspiring guidance, constructive suggestions and advice during my work, which will be an unforgettable experience during my all life.

Finally, I wish to thank my parents for their support and encouragement throughout my study.

BUDAPEST UNIVERSITY OF TECHNOLOGY AND ECONOMICS

Abstract

Faculty of Mechanical Engineering
Department of Applied Mechanics

Mechanical Engineering

Separation of in-plane fracture modes by four equivalent single layers

by Balázs KISS

By using more and more fiber reinforced thermoset polymer composites the need of undestanding their mechanical description becomes inevitable in the engineering life. Because of the direction dependent material properties they offer great freedom to the designers, although, their complex mechanical behaviour hides some drawbacks, as well. Comparing to the other commonly used heterogeneous engineering materials, very different modes of failure can take place. One of the most distinctive and typical form of these damages is the so-called interlaminar fracture or delamination. During this phenomenon the laminated layers get separated from each other causing significant loss of mechanical properties. Even nowadays, it is a pioneering research topic from fracture mechanics and material science point of view, as well.

In this thesis work I deal with those kind of mechanical models which are applicable to describe laminated composite beams. New types of model are developed and compared to each other. Along the thickness of the beam the displacement field is approximated with higher-order polynomials applying semi-layerwise technique. The equilibrium equations are derived by using the virtual work principle [1, 5, 7]. Solving the system of ODEs and utilizing the more accurate displacement and stress field around the crack tip the application of the J-integral becomes feasible. According to the basic definition of this integral the energy release rate, which is the fundamental quantity of the linear elastic fracture mechanics, can be calculated. Reaching the critical value of this parameter in a given material the delamintaion propagates and the layers separate from each other [2]. Furthermore, by using the J-integral more accurate and exact in-plane fracture mode partitioning becomes achievable (in the case of beam specimens mode-I and mode-II can appear) comparing to the previously published solutions and models in the literature [4, 9, 10, 11, 12].

For my grandparents, who had never had possibility of learning.

Contents

Chapter 1

Introduction

In this chapter those kind of definitions are introduced which are indispensable to understand this final report. It briefly deals with the basic concepts of fracture and composite mechanics, and furthermore, introduces one of the most distinctive form of damages in fiber reinforced polymer composites.

1.1 Basics of fracture mechanics

In agreement with the linear elastic fracture mechanics approach, the given cracked body is essentially linear elastic. Crack initiation and propagation is governed by the so-called "energy release rate". According to the formulation, the energy release rate is the change in the total potential energy Π of the linear elastic system with respect to the inceremental increase in the crack area dA:

$$G = -\frac{d\Pi}{dA} \,. \tag{1.1}$$

The total potential energy in a given elastic body is defined as:

$$\Pi = U - W, \tag{1.2}$$

where U is the sum of the stored elastic strain energy and W is the work of external forces [2, 6]. This energy based definition, which was originally proposed by Irwin in 1956, supplementing with the Griffith's criterion is already suitable to handle the existing singularity

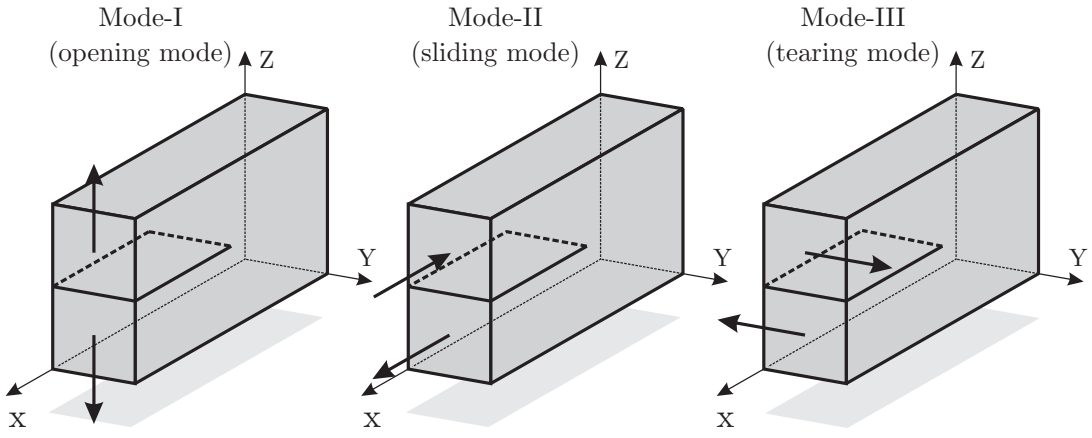

FIGURE 1.1: Basic fracture modes in linear elastic fracture mechanics.

nature of the stress field in the small vicinity of crack tips. According to the Griffith's criterion, crack initiation, or propagation can occur only if the energy release rate reaches the G_c critical value. Similarly to the Young's modulus or Poisson's ratio, it can be discussed and handled as a material property [2]. For the determination of G_c some experimentally recorded quantities, such as critical load and displacement are necessary. The three basic fracture modes are shown in Figure 1.1. In case of mode-I, where the principal load is applied normal to the crack plane, the crack tends to open. By applying forces parallel to the crack plane sliding can appear. It is mode-II. Mode-III refers to out-of-plane shear causing some kind of tearing. A cracked body can be loaded in any of these modes, or a combination of two or three modes [6].

1.2 Delamination in composite structures

Composites are multicomponent, multiphase, inhomogeneous materials consisting of high strength, high modulus reinforcement phase and tough but stiff matrix phase. Strong adhesion between the two phases, which remains relaiable even at high strains and stresses, is essential [14]. A typical tensile test of polymer composite and its components are depicted by Figure 1.2. As can be seen, the breaking strength of the composite becomes much higher than the original matrix has, furthermore, the breaking strain is mainly determined by the fiber reinforcement causing significant increase of the Young's modulus. One of the main advantages, beside the high strength despite low density, is that load bearing capacity can be fitted to the loading direction. This type of materials has uniquely tailorable mechanical properties, not to mention some other functional and operational benefits, like corrosion,

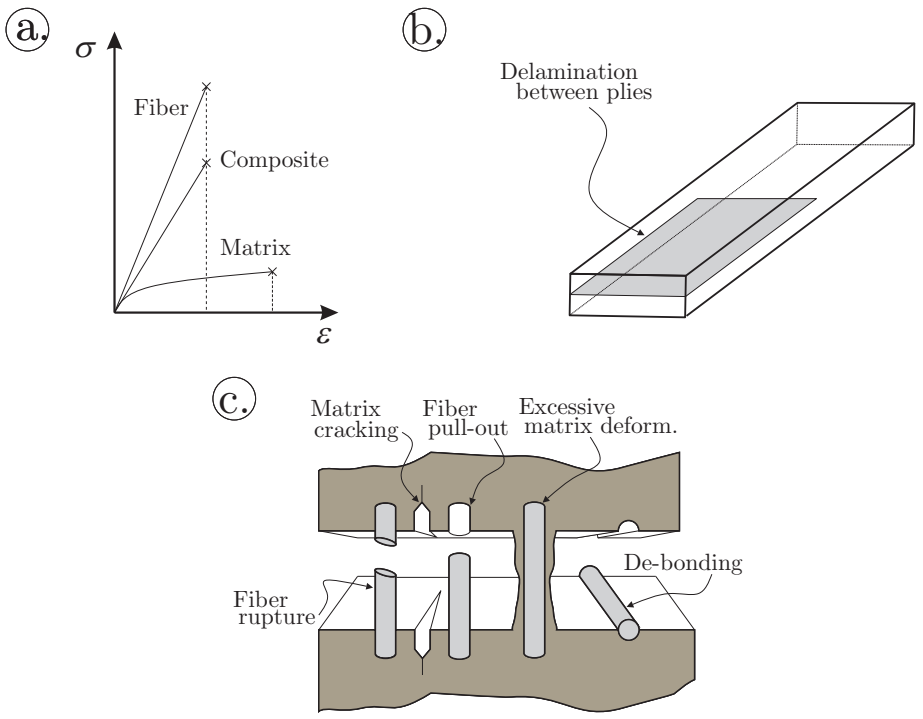

FIGURE 1.2: Tensile test of polymer composite and its components (a). Possible failure mechanism of composite materials (b-c).

chemical and fatigue resistance [14]. However, composite materials are susceptible to various and quite complicated failure mechanisms, as well. As it is illustrated by Figure 1.2, fiber rupture, matrix cracking, fiber pull-out, fiber-matrix de-bonding, excessive matrix deformation and among others, due to the weakening of interface layer between the laminated plies, interlaminar fracture or delamination can occur, which is the main object of this report [6, 14]. This unavoidable and critical interlaminar failure behavior inspires us to find mechanical models to describe and, if it is possible, delay or prevent delamination in order to increase the life and load bearing capability of the laminated structures.

Application of linear fracture mechanics is one of the possible way of describing delaminated structures. The previously introduced G_c critical energy release rate value is applicable to characterize the interface layer between two composite plies.

1.3 Main aims and analysis methods

As it was already mentioned, application of linear elastic fracture mechanics makes possible to describe and characterize a given interface strength between two composite plies by using G_c value. Similarly to metals, in order to determine this material parameter and to investigate the failure process in composites, experimental investigations have to be performed. Generally, the fracture tests are carried out on different type of pre-cracked specimens including mode-I, mode-II, mixed-mode I/II, mode-III, mixed-mode I/III, mixed-mode II/III and mixed-mode I/II/III test by utilizing basic geometries like beams and plates [5, 6]. However, in order to determine the energy release rate, mechanical model has to be applied.

Previously, in the literature, many models were developed based on Euler-Bernoulli hypothesis [9, 10, 11]. According to this hypothesis, the cross sections of the beam are assumed to remain planar and normal to the tangent of beam flexure. Thus, the assumed dipslacement vector field can be written in the following form:

$$\boldsymbol{u}(x,z) = \begin{pmatrix} u \\ 0 \\ w \end{pmatrix}, \qquad u(x,z) = u_0(x) - z\frac{\partial w}{\partial x}, \qquad w(x) = w_0(x), \tag{1.3}$$

where there are two independent parameters: u_0 is the membrane displacement and w is the transverse deflection of the bent beam. The rotation of the cross section, as it is illustrated by Figure 1.3, is approximated by the derivative of the deflection. However, using this theorem, the effect of transverse shear cannot be taken into account [1].

To solve this contradiction and to increase the accuracy of beam models researchers were encouraged and inspired to introduce novel, higher order beam theorems. The first-order shear deformable beam theory (FSDT) assumes independent $\theta(x)$ rotation about the Y axis:

$$\boldsymbol{u}(x,z) = \begin{pmatrix} u \\ 0 \\ w \end{pmatrix}, \qquad u(x,z) = u_0(x) + \theta(x)z, \qquad w(x) = w_0(x). \tag{1.4}$$

By generalization of the FSDT displacement field in thickness direction the higher-order theories, second- and third-order shear deformabe theories (SSDT-TSDT), can be obtained:

$$u(x,z) = u_0(x) + \theta(x)z + \phi(x)z^2 + \lambda(x)z^3..., \tag{1.5}$$

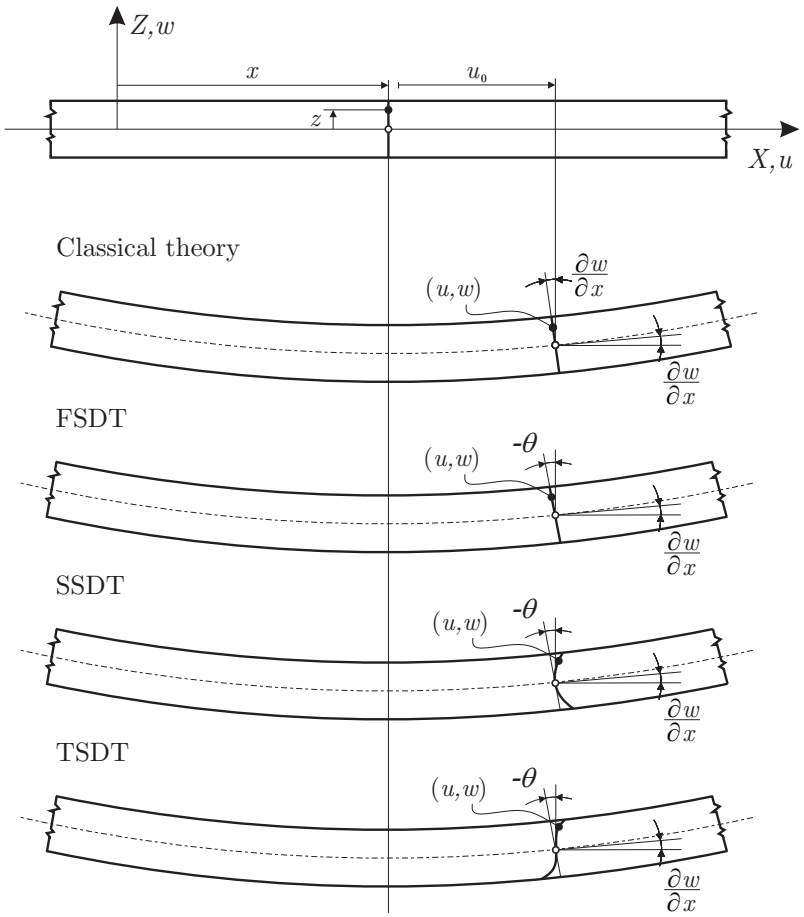

FIGURE 1.3: The deformation of material line of a beam on the x - z plane in accordance with the different beam theories.

where $\theta(x)$ denotes the angle of rotation (or first-order term), $\phi(x)$ represents the second-order term (SSDT) and $\lambda(x)$ describes the third-order term (TSDT). The assumed displacement field in each theory is also shown in Figure 1.3.

In the following, by utilizing the basic ideas of higher-order beam theories, novel beam models are developed and used to decribe the displacement and stress field more accurately around the cract tip in delaminated composite specimens. Using the concepts of semi-layerwise plate model [5], the so-called semi-layerwise beam model is defined and used to predict mechanical behavior of delaminated composite beams in the case of mode-I, mode-II and mixed-mode I/II interlaminar fracture conditions. In order to calculate the energy release rate and to separate it into mode-I and mode-II parts, the J-integral is applied. Using the definition of this integral and by decomposing the calculated strain and stress fields into symmetric and antisymmetric parts with respect to the delamination plane, more accurate and exact mode partitioning becomes achievable compared to the previously published solutions in the litarature, which are mostly based on Euler-Bernoulli beam theory [4].

1.4 Orthotropic and transversely isotropic materials

One of the main advantages of using composite materials is that these materials have uniquely tailorable material properties. Using different lay-up sequences and designs the load-bearing capacity can be modified in each directions, thus obtaining generally anisotropic materials. By writing the σ stress and ε strain tensors into vectorial forms, the Hooke's law can be formulated as:

$$\sigma = C\varepsilon \quad or \quad \varepsilon = S\sigma, \qquad S^{-1} = C, \qquad S^T = S, \tag{1.6}$$

where C is the reduced stiffness matrix and S is the compliance matrix. These are full 6x6 matrices, but they are symmetric, as well, requiring 21 engineering constants and describing several coupling between different deformations [3].

Nevertheless, if we look at only one ply in its own material coordinate system, it mostly behaves like orthotropic and transversely isotropic material which significantly reduces the necessary number of material constants. In the case of orthotropic material behavior, as it is illustrated by Figure 1.4, there are three mutually orthogonal material planes. An important feature of orthotropic material behavior is that there is no coupling between simple tensions and shears. If σ_1 is applied in X_1 direction, then shear strain does not appear. The number of independent constants is reduced to 9, and S compliance matrix can be written in the following form:

$$S = \begin{bmatrix} 1/E_{11} & -\nu_{21}/E_{22} & -\nu_{31}/E_{33} & 0 & 0 & 0 \\ -\nu_{12}/E_{11} & 1/E_{22} & -\nu_{32}/E_{33} & 0 & 0 & 0 \\ -\nu_{13}/E_{11} & -\nu_{23}/E_{22} & 1/E_{33} & 0 & 0 & 0 \\ 0 & 0 & 0 & 1/G_{23} & 0 & 0 \\ 0 & 0 & 0 & 0 & 1/G_{13} & 0 \\ 0 & 0 & 0 & 0 & 0 & 1/G_{12} \end{bmatrix}, \tag{1.7}$$

where $E_{11}, E_{22}, E_{33}, G_{12}, G_{13}, G_{23}, \nu_{12}, \nu_{13}, \nu_{23}$ denote the necessary engineering constants [3].

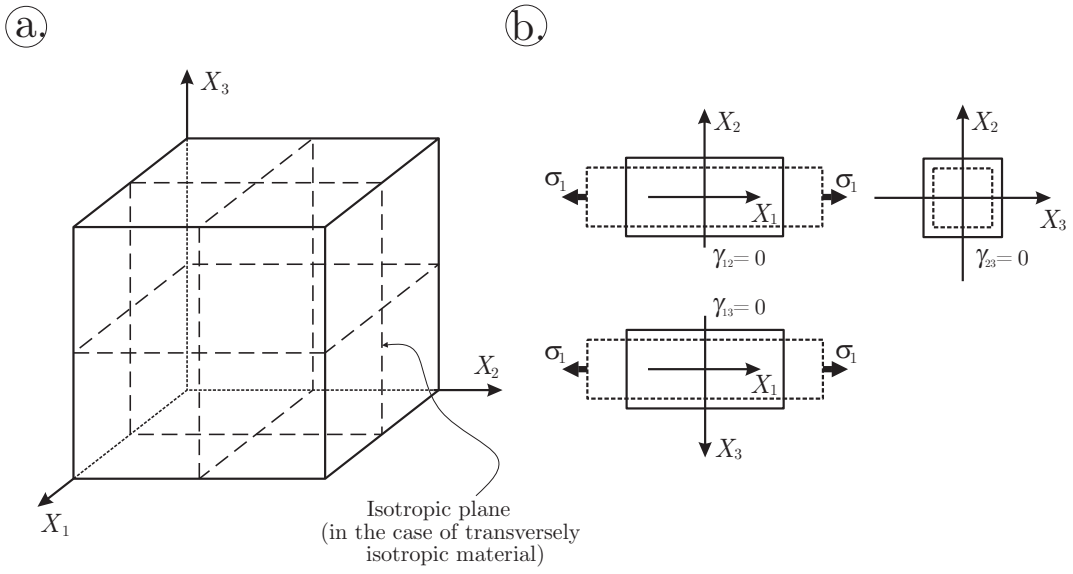

FIGURE 1.4: The material symmetry planes (a) and tension without any tension-shear coupling (b).

The next level of material symmetry is the tranversely isotropic material, which has 5 independent constants. Supposing this kind of material behavior requires that one of the three material symmetry planes has to be isotropic plane, as well. This case is also depicted in Figure 1.4. The stress-strain relation for a tranversely isotropic material takes the form:

$$\boldsymbol{S} = \begin{bmatrix} 1/E_{11} & -\nu_{21}/E_{22} & -\nu_{21}/E_{22} & 0 & 0 & 0 \\ -\nu_{12}/E_{11} & 1/E_{22} & -\nu_{32}/E_{22} & 0 & 0 & 0 \\ -\nu_{12}/E_{11} & -\nu_{23}/E_{22} & 1/E_{22} & 0 & 0 & 0 \\ 0 & 0 & 0 & 2(1+\nu_{23})/E_{22} & 0 & 0 \\ 0 & 0 & 0 & 0 & 1/G_{13} & 0 \\ 0 & 0 & 0 & 0 & 0 & 1/G_{13} \end{bmatrix}, \tag{1.8}$$

where the independent constants according to the Figure 1.4 are $E_{11}, E_{22}, G_{13}, \nu_{12}, \nu_{23}$ [3].

1.4.1 Plane stress reduced constitutive relations

According to [1], in case of beams and plates, which are modeled by using their middle plane, plane-stress condition can be assumed. The stress-strain relations of an orthotropic body under plane stress state can be written as:

$$\begin{pmatrix} \sigma_1 \\ \sigma_2 \\ \tau_{12} \end{pmatrix} = \begin{bmatrix} E_{11}/(1-\nu_{21}\nu_{12}) & \nu_{21}E_{11}/(1-\nu_{21}\nu_{12}) & \\ \nu_{12}E_{22}/(1-\nu_{21}\nu_{12}) & E_{22}/(1-\nu_{21}\nu_{12}) & \\ 0 & 0 & G_{12} \end{bmatrix} \begin{pmatrix} \varepsilon_1 \\ \varepsilon_2 \\ \gamma_{12} \end{pmatrix}, \tag{1.9}$$

furthermore, $\sigma_3 = \tau_{13} = \tau_{23} = 0$. In case of beam, only one term remains:

$$\sigma_1 = \frac{E_{11}}{(1-\nu_{21}\nu_{12})}\varepsilon_1. \tag{1.10}$$

A quite important property of the higher-order beam (and plate) theories is that by taking into account tranverse shear stress does not disturb the plane stress assumptions of the

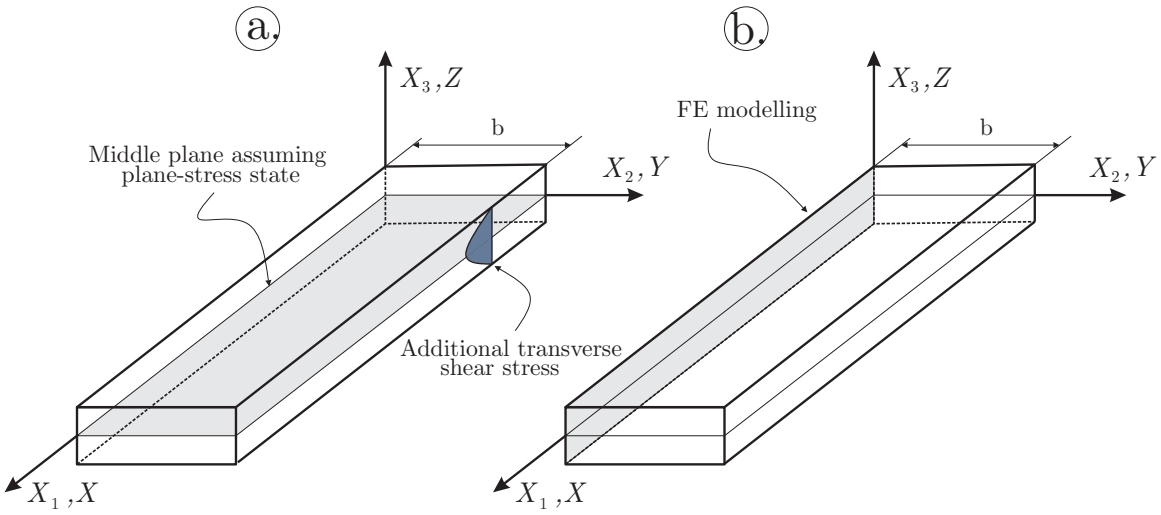

FIGURE 1.5: Comparison of the analytical (a) and numerical FE model (b) of the problem.

stress field. The appearing shear effect is treated separately from these conditions. Referring again to [1], and as it is shown by Figure 1.5, the transverse shear stress is calculated as an additional stress term:

$$\tau_{13} = G_{13}\gamma_{13}. \tag{1.11}$$

Although, applying numerical modelling, by e.g. plane elements, beams are generally not modelled by their middle plane. Instead of that, the $X_1 - X_3$ plane is used to describe the stress field by using plane stress conditions, again.
For the sake of simplicity, in the remaining discussion the material (X_1, X_2, X_3) coordinates and the global (X, Y, Z) coordinates are exactly the same.

1.5 Evaluation techniques in the literature

These evaluation methods in the literature, apart form the virtual crack closure technique (VCCT), are basically based on the classical Euler-Bernoulli beam theory. These methods are used in the following discussion as reference results to compare the newly developed in-plane separation technique.

1.5.1 Williams, Bruno-Greco and Luo-Tong solutions

These solutions are suitable to describe in-plane mode partitioning in composite specimens containing two or even any kind of orthotropic plies. First of all, it is important to highlight and emphasize, the neutral planes of the portions are not necessarily coincide with the reference planes anymore. As it is illustarted by Figure 1.6, according to the actual structure of the laminated plies, the neutral planes are shifted or can be shifted. By making the B_{11} coupling stiffnes with respect to the local reference planes equal to zero, each and every case the neutral plane can be found. Generally, this can be expressed as:

$$B_{11} = b\frac{1}{2}\sum_{m=1}^{N_l} \overline{C}_{11}^{(m)}([z_{m+1} + t_s]^2 - [z_m + t_s]^2) = 0, \tag{1.12}$$

where t_s denotes the unknown offset between the neutral and local reference plane and the other terms are equivalent with the previous notations used in Eqs.(2.15) and (2.19). Solving this equation, separately for the undelaminated and delaminated portions, t_s, t_{st} and t_{sb} can be obtained. Thus the bending stiffnesses, taking into account the offset, can be calculated as:

$$D_{11}^{(undel)} = b\frac{1}{3}\sum_{m=1}^{N_l} \overline{C}_{11}^{(m)}([z_{m+1} - t_s]^3 - [z_m - t_s]^3), \tag{1.13}$$

furthermore:

$$D_{11}^{(top)} = b\frac{1}{3}\sum_{m=1}^{N_l^{(top)}} \overline{C}_{11}^{(m)}([z_{m+1}^{(top)} - t_{st}]^3 - [z_m^{(top)} - t_{st}]^3), \tag{1.14}$$

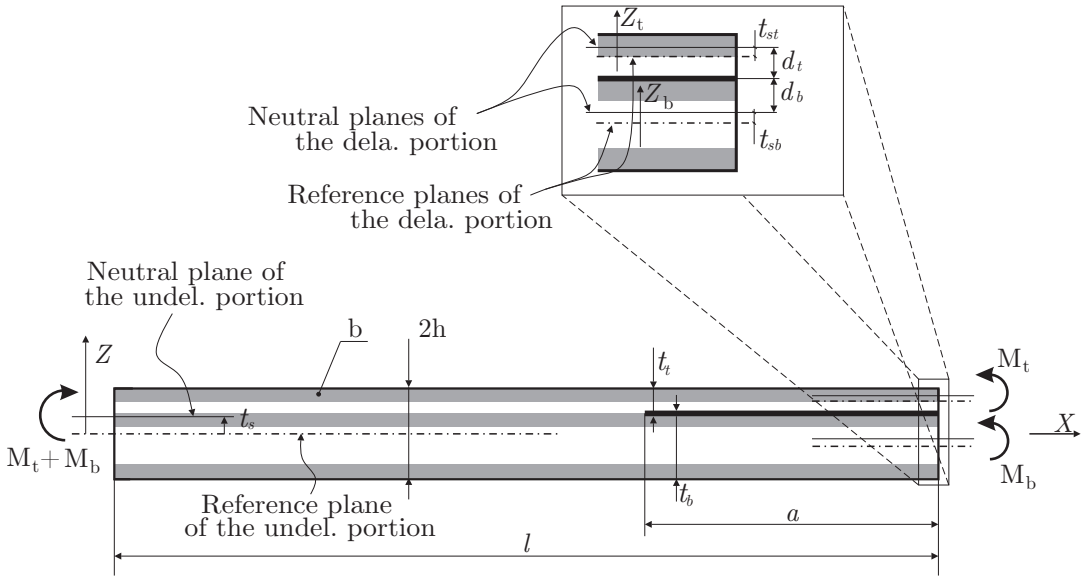

FIGURE 1.6: General loading scenario and the offset of the neutral planes in the case of composite specimen with arbitrary structure of orthotropic plies.

and:

$$D_{11}^{(bot)} = b\frac{1}{3}\sum_{m=1}^{N_l^{(bot)}} \overline{C}_{11}^{(m)}([z_{m+1}^{(bot)} - t_{sb}]^3 - [z_m^{(bot)} - t_{sb}]^3). \tag{1.15}$$

where $(undel)$ refers to the undelaminated protion, and $(top), (bot)$ superscripts to the top and bottom sub-laminates of the delaminated portions, separately. Utilizing the calculated stiffnesses the strain energy of the system can be obtained:

$$U = \frac{1}{2}\Big(\frac{(M_t + M_b)^2(l-a)}{D_{11}^{(undel)}} + \frac{M_t^2 a}{D_{11}^{(top)}} + \frac{M_b^2 a}{D_{11}^{(bot)}}\Big), \tag{1.16}$$

where M_t and M_b represent the tip bending moments on the top and bottom sub-laminates. And finally, the G_T total energy release rate of the system, according to the Griffith-Irwin formula [2], can be determined as:

$$G_T = \frac{1}{b}\frac{dU}{da}. \tag{1.17}$$

Williams curvature based solution

To carry out energy release rate partition, the bending moments can be decomposed into their mode components:

$$\begin{aligned} M_t &= M_I + M_{II}, \\ M_b &= \alpha M_I + \psi M_{II}, \end{aligned} \tag{1.18}$$

where M_I denotes that part of the bending moment which contributes to mode-I and M_{II} represents that part which contributes to mode-II energy release rate. Furthermore, α and ψ

are unknown parameters which have to be determined by some assumptions. In order to make mode separation possible, Williams proposed to use curvature equality [9]. Meaning, in the case of pure mode-II tests, the curvatures of the sub-laminate deflections are equal to each other along the delamination length. By assuming pure mode-II loading scenario:

$$\begin{aligned} M_I = 0 \longrightarrow\ & M_t = M_{II}, \\ & M_b = \psi M_{II}, \end{aligned} \tag{1.19}$$

and by expressing the curvatures of the sub-laminate deflections:

$$\frac{M_t}{D_{11}^{(top)}} = \frac{M_b}{D_{11}^{(bot)}} \longrightarrow \frac{M_{II}}{D_{11}^{(top)}} = \frac{\psi M_{II}}{D_{11}^{(bot)}}, \tag{1.20}$$

from which the ψ unknown parameter can be determined as:

$$\psi = \frac{D_{11}^{(bot)}}{D_{11}^{(top)}}. \tag{1.21}$$

In order to determine α, everything has to be substituted back into Eq.(1.17). Hereby, one important property of the G_T is utilized:

$$G_T = G_I + G_{II}, \tag{1.22}$$

which is also crucial from the point of mode mixity [2]. Thus, the total energy release rate cannot contain $M_I M_{II}$ mixed product terms. By collecting the mixed product term and, in order to vanish, make it equal to zero:

$$M_I M_{II}: \quad \left(\frac{(1 + D_{11}^{(bot)}/D_{11}^{(top)})(1+\alpha)}{bD_{11}^{(undel)}} + \frac{1}{bD_{11}^{(top)}} + \frac{\alpha}{bD_{11}^{(bot)}} \right) M_I M_{II} = 0, \tag{1.23}$$

this leads to:

$$\alpha = -1. \tag{1.24}$$

Imposing these conditions, the in-plane mode partitiong can already be accomplished by:

$$M_I: \ G_I = \frac{1}{2}\left(\frac{bD_{11}^{(top)} D_{11}^{(bot)}}{(D_{11}^{(top)} + D_{11}^{(bot)})} \right) M_{II}^2 \qquad M_{II},: \ G_{II} = \frac{1}{2}\left(... \right) M_I^2. \tag{1.25}$$

Bruno-Greco strain based solution

According to this solution, pure mode-I condition produces the same strain at the delamination tip. By assuming this type of loading scenario, we have:

$$\begin{aligned} M_{II} = 0 \longrightarrow\ & M_t = M_I, \\ & M_b = \alpha M_I, \end{aligned} \tag{1.26}$$

and by using the strain based condition the following relation for α is obtained :

$$-\frac{M_t}{D_{11}^{(top)}}d_t = \frac{M_b}{D_{11}^{(bot)}}d_b \longrightarrow -\frac{M_I}{D_{11}^{(top)}}d_t = \frac{\alpha M_I}{D_{11}^{(bot)}}d_b, \tag{1.27}$$

where d_t and d_b denote the distance of the neutral planes from the delamination by referring again to Figure 1.6. Furthermore, according to the previously introduced algorithm, ψ is obtained by imposing that the mixed-term must be zero. This solution can be found in the literature as Bruno-Greco solution [10].

Luo-Tong strain based solution

Based on deformation analysis for a cracked laminate subjected to bending moments Luo and Tong proposed a new mode partition equation. Similary to Bruno and Greco, they assumed that the pure mode-I condition is produced by the same strain at the delamination tip. Although, in order to express this strain at the delamination front, the curvature of the undelaminated part is also taken into account meaning significant contribution compare to the beforehand discussed evaluation techniques. By assuming pure mode-I loading scenario:

$$\begin{aligned} M_{II} = 0 \longrightarrow\ & M_t = M_I, \\ & M_b = \alpha M_I, \end{aligned} \tag{1.28}$$

and by using the strain based condition proposed by Luo-Tong the relation for α can be formulated as:

$$-\frac{1}{2}\left(\frac{M_t}{D_{11}^{(top)}} + \frac{M_t + M_b}{D_{11}^{(undel)}}\right)d_t = \frac{1}{2}\left(\frac{M_b}{D_{11}^{(bot)}} + \frac{M_t + M_b}{D_{11}^{(undel)}}\right)d_b, \tag{1.29}$$

resulting in the following condition:

$$-\frac{1}{2}\left(\frac{M_I}{D_{11}^{(top)}} + \frac{M_I + \alpha M_I}{D_{11}^{(undel)}}\right)d_t = \frac{1}{2}\left(\frac{\alpha M_I}{D_{11}^{(bot)}} + \frac{M_I + \alpha M_I}{D_{11}^{(undel)}}\right)d_b. \tag{1.30}$$

Basically, by using this technique, we simply calculate the curvature at the crack tip as an average value of the delaminated and the undelaminated portions. Finally, according to the previously utilized algorithm, ψ can be expressed by imposing that the mixed-term must be zero [11].

1.5.2 VCCT

The virtual crack closure technique (VCCT) for determination of energy release rate has been proposed for 40 years ago. According to it, as it is depicted by Figure 1.7, the so-called "Davidson-mesh" has to be built up in the small vicinity of the delamination front. By reading out the F_{ki} nodal forces and u_{ki} nodal displacements of the k^{th} node, the energy relase rates become:

$$G_i = \frac{1}{2b\Delta c}\sum_{k=1}^{2} F_{ki}u_{ki} \qquad (i = 1,2,3), \tag{1.31}$$

where i refers to the mode type, b and Δc represent the geometry of the applied mesh. This technique is equally applicable for numerical calculation of mode-I, mode-II and mode-III energy relase rates by using respectively 2D or 3D elements.

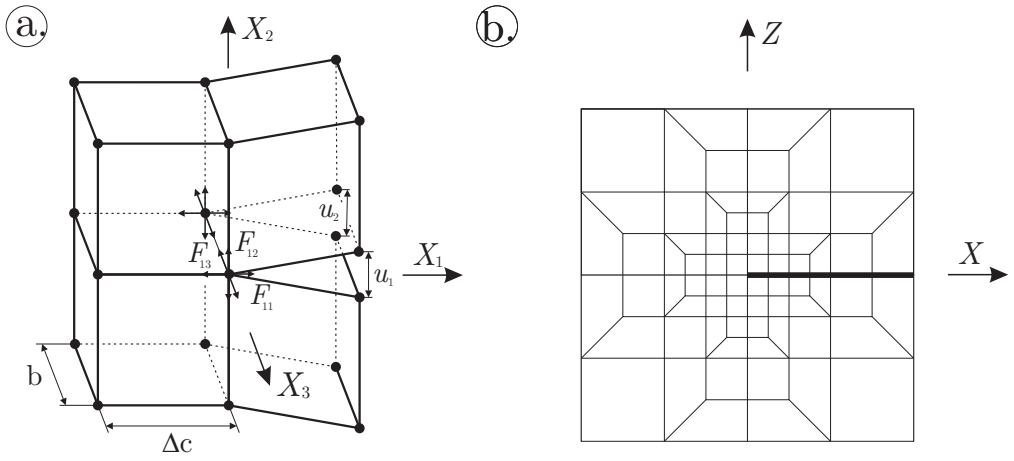

FIGURE 1.7: The VCCT technique (a) and the special Davidson-mesh around the crack tip (b).

Chapter 2

The basic equations of delaminated composite beams

In this chapter the basic equations of delaminated composite beams are presented. The formulations are based on the so-called "semi-layerwise" modeling technique [5]. The invariant form of the equilibrium equations, separately for the delaminated and undelaminated portion, are derived by using the virtual work principle [1].

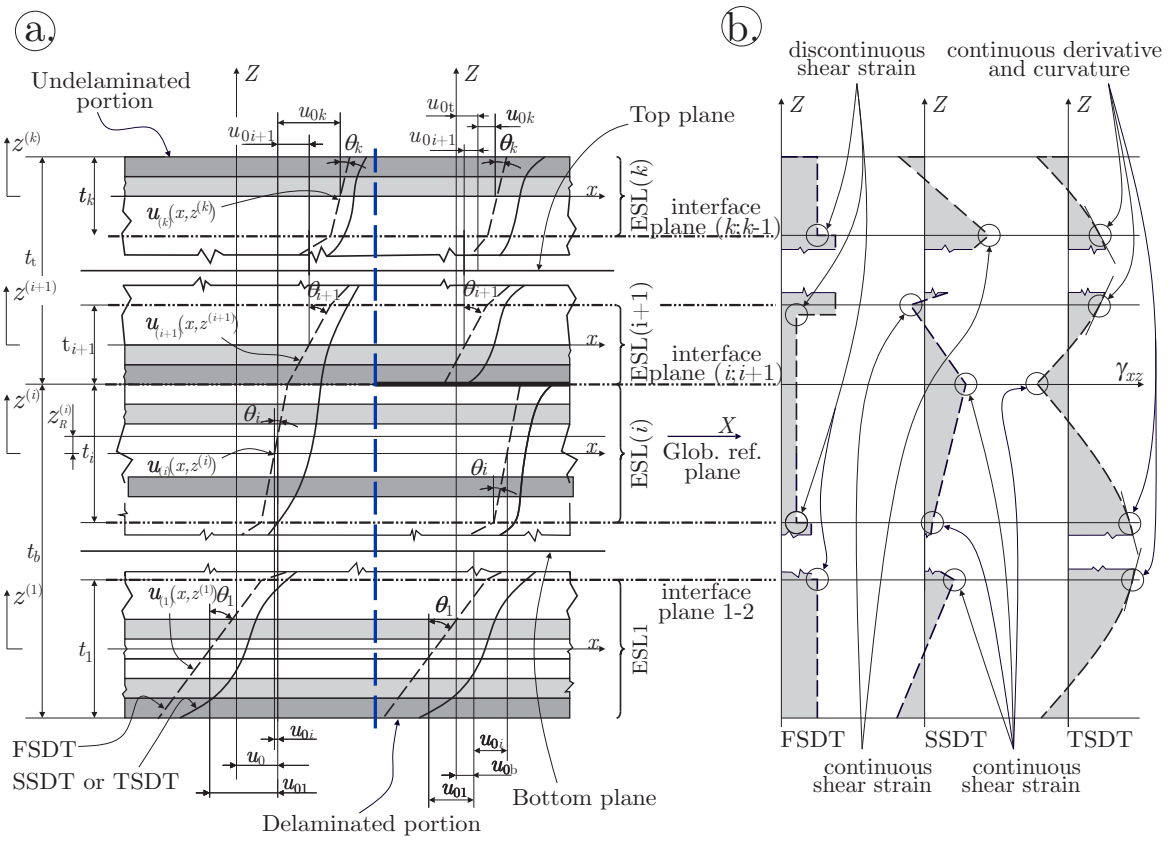

FIGURE 2.1: Cross sections and deformation of the top and bottom beam elements of a delaminated beam in the $X-Z$ plane (a) and distributions of the transverse shear strain by different theories (b).

2.1 Semi-layerwise beam model

As it is shown in Figure 1.2 (c), if a delamination occurs in a composite beam it separates the beam into a top and bottom sub-laminates. In order to deal with this phenomena the model has to be divided into top and bottom parts, too. These parts are further divided into equivalent single layers (in the following "ESL"), which are represented by Figure 2.1. This method is the so-called "semi-layerwise" technique. According to the definition of semi-layerwise beam model, which was originally defined for composite plates, if a laminated composite beam with N_l number of layers is modelled by N_{ESL} number of equivalent single layers and $N_{ESL} < N_l$ than the model is called semi-layerwise beam model. In this case the stiffness parameters of each ESL has to be calculated with respect to the local reference planes of the ESLs [5].

Figure 2.1 shows the transition section between the delaminated and undelaminated portions of the composite beam in the X-Z plane, as well. The transverse splitting by using blue dashed line highlights that fact the undelaminated and delaminated regions are described by different mathematical functions. The two coordinate systems are to depict the displacement parameters in the different portions, separately. The general case involves k number of ESLs applied through the whole thickness of the beam. For each and every ESL the displacement field can be written in the following form:

$$\begin{aligned} u_{(i)}(x, z^{(i)}) &= u_0(x) + u_{0i}(x) + \theta_i(x) z^{(i)} + \phi_i(x)[z^{(i)}]^2 + \lambda_i(x)[z^{(i)}]^3, \\ w_{(i)}(x) &= w_{(i)}(x), \end{aligned} \tag{2.1}$$

where i denotes the index of actual ESL, $z^{(i)}$ is the local thickness coordinate of the i^{th} ESL and always coincides with the local midplane, u_0 is the global, u_{0i} is the local membrane displacements, θ denotes the rotation of the cross section about the Y axes, ϕ means the second-order, and λ expresses the third-order terms in the assumed displacement fields. Moreover, $w_{(i)}$ represents the separate transverse deflection function. Eq. (2.1) is applied equally to the undelaminated and delaminated portions, as well. The displacement functions of FSDT and SSDT can be obtained by substituting $\phi = 0$ and $\lambda = 0$ into the Eq. (2.1), respectively. The displacement field given by Eq.(2.1) is associated to each ESL [5].

2.2 The system of exact kinematic conditions

The kinematic continuity of the displacement fields between the contiguous ESLs is specified by using the sytem of exact kinematic conditions [5]:

$$(u_{(i)}, w_{(i)})\Big|_{z^{(i)}=t_i/2} = (u_{(i+1)}, w_{(i+1)})\Big|_{z^{(i+1)}=-t_{i+1}/2}, \tag{2.2}$$

where t_i is the thickness of the specified ESL. On the other hand, it is important to highlight and indicate, $w_{(i)}$ does not depend on $z^{(i)}$ coordinate. It means that each $w_{(i)}$ is replaced with simple w function through the whole thickness. The second condition restricts the u_0 global membrane displacement at the reference plane of the actual region. If it is located in

the i^{th} layer and the coordinate of the global reference plane is z_R^i within this i^{th} coordinate system, then the condition can be written as:

$$u_{(i)}\Big|_{z^{(i)}=z_R^{(i)}} - u_0 = 0. \tag{2.3}$$

Eqs.(2.2)-(2.3) are already sufficient to develop semi-layerwise model for the FSDT. If the SSDT or TSDT is applied, then shear strain continuities at the interface planes can be or have to be introduced. In accordance with Figure 2.1(b), these conditions are expressed as:

$$\gamma_{xz(i)}\Big|_{z^{(i)}=t_i/2} = \gamma_{xz(i+1)}\Big|_{z^{(i+1)}=-t_{i+1}/2}. \tag{2.4}$$

For the TSDT theory two more types of kinematic conditions have to be imposed. These are the derivatives and the curvatures of the shear strain between the interfaces:

$$\frac{\partial\gamma_{xz(i)}}{\partial z^{(i)}}\Big|_{z^{(i)}=t_i/2} = \frac{\partial\gamma_{xz(i+1)}}{\partial z^{(i+1)}}\Big|_{-z^{(i+1)}=t_{i+1}/2}, \tag{2.5}$$

and:

$$\frac{\partial^2\gamma_{xz(i)}}{\partial\left(z^{(i)}\right)^2}\Big|_{z^{(i)}=t_i/2} = \frac{\partial^2\gamma_{xz(i+1)}}{\left(\partial z^{(i+1)}\right)^2}\Big|_{-z^{(i+1)}=t_{i+1}/2}. \tag{2.6}$$

These conditions can be imposed to the undelaminated and delaminated portions of the beam, as well. In Eq.(2.1) the displacement fields are modified in order to satisfy Eq.(2.2)-(2.6). By using the FSDT, SSDT and TSDT theories the displacement functions can be expressed in the following, compact form [5]:

$$u_{(i)} = u_0 + \left(K_{ij}^{(0)} + K_{ij}^{(1)}z^{(i)} + K_{ij}^{(2)}[z^{(i)}]^2 + K_{ij}^{(3)}[z^{(i)}]^3\right)\psi_j, \quad i = 1..k, \tag{2.7}$$

where K_{ij} is the displacement multiplicator matrix and related exclusively to the geometry (thicknesses of the ESLs), i refers to the ESL number, the summation index j defines the components in $\boldsymbol{\psi_p}$, which is the vector of primary parameters. Eq.(2.7) can be obtained by using parameter elimination. Certain parameters of the displacement functions can be eliminated by the previously introduced system of exact kinematic conditions. Using the remaining (primary) parameters each and every eliminated (secondary) parameters can be expressed [5]. Theoretically, selecting the necessary primary parameter is almost arbitrary, but for instance, the local membrane displacements are typically secondary, the global membrane displacements are typically primary parameters. It is important to highlight the size and elements number of the $\boldsymbol{\psi_p}$ depend on the applied theory, the number of ESLs and the number of imposed conditions.

2.3 Virtual work principle and constitutive equations

If the displacement field is known, assuming small displacements, the strain field in an elastic beam can be obtained by the following equations:

$$\varepsilon_{x(i)} = \frac{\partial u_{(i)}}{\partial x}, \qquad \gamma_{xz(i)} = \frac{\partial u_{(i)}}{\partial z^{(i)}} + \frac{\partial w_{(i)}}{\partial x}, \tag{2.8}$$

where ε_x is the normal strain in the x-direction, and γ_{xz} is the shear strain. Thus, the strains become:

$$\varepsilon_{x(i)} = \varepsilon^{(0)}_{x(i)} + z^{(i)} \cdot \varepsilon^{(1)}_{x(i)} + [z^{(i)}]^2 \cdot \varepsilon^{(2)}_{x(i)} + [z^{(i)}]^3 \cdot \varepsilon^{(3)}_{z(i)}, \tag{2.9}$$

and:

$$\gamma_{xz(i)} = \gamma^{(0)}_{xz(i)} + z^{(i)} \cdot \gamma^{(1)}_{xz(i)} + [z^{(i)}]^2 \cdot \gamma^{(2)}_{xz(i)}. \tag{2.10}$$

To derive the governing equations the virtual work principle can be applied [1]:

$$\int_{T_0}^{T_1} (\delta U - \delta W_F) dt = 0, \quad \delta U = \sum_i \delta U_{(i)}, \quad \delta W_F = \sum_i \delta W_{F(i)}, \tag{2.11}$$

where U denotes the strain energy, W_F represents the work of external forces and t is the time. The virtual strain energy of the laminated composite beam sytem for the i^{th} ESL can be expressed as:

$$\delta U_{(i)} = \int_V \boldsymbol{\sigma}_{(i)} : \delta \boldsymbol{\varepsilon}_{(i)} dV = \int_{(l)} \left\{ \int_0^b \int_{-t_i/2}^{t_i/2} (\sigma_{x(i)} \delta \varepsilon_{x(i)} + \tau_{xz(i)} \delta \gamma_{xz(i)}) dz^{(i)} dy \right\} dx, \tag{2.12}$$

where $\sigma_{(i)}$ is the stress tensor, $\delta \boldsymbol{\varepsilon}_{(i)}$ is the virtual strain tensor of the i^{th} ESL and l denotes the domain of the beam. Taking back the strain fields into Eq.(2.12), the following can be obtained:

$$\begin{aligned} \delta U_{(i)} = \int_{(l)} \Bigg\{ \int_0^b \int_{-t_i/2}^{t_i/2} \Big[& \sigma_{x(i)} \left(\delta \varepsilon^{(0)}_{x(i)} + y^{(i)} \cdot \delta \varepsilon^{(1)}_{x(i)} + [z^{(i)}]^2 \cdot \delta \varepsilon^{(2)}_{x(i)} + [z^{(i)}]^3 \cdot \delta \varepsilon^{(3)}_{x(i)} \right) \\ & + \tau_{xz(i)} \left(\delta \gamma^{(0)}_{xz(i)} + z^{(i)} \cdot \delta \gamma^{(1)}_{xz(i)} + [z^{(i)}]^2 \cdot \delta \gamma^{(2)}_{xz(i)} \right) \Big] dz^{(i)} dy \Bigg\} dx. \end{aligned} \tag{2.13}$$

Furthermore, the constitutive equation has to be used to continue the derivation. The constitutive equation for orthotropic and transversely ispotropic materials has already been discussed through Eq.(1.10)-(1.11). As a reminder, in this final project report, the material coordinates and the global coordinates are exactly the same for the sake of simplicity. Thus

the constitutive relations can be formulated in the following form [1]:

$$\begin{aligned}\begin{pmatrix}\sigma_x\\ \tau_{xz}\end{pmatrix}_{(i)} = \overline{\boldsymbol{C}}^{(m)}_{(i)}\begin{pmatrix}\varepsilon_x\\ \gamma_{xz}\end{pmatrix}_{(i)} &= \begin{bmatrix}\overline{C}_{11} & 0\\ 0 & \overline{C}_{55}\end{bmatrix}^{(m)}_{(i)}\begin{pmatrix}\varepsilon_x\\ \gamma_{xz}\end{pmatrix}_{(i)}\\ &= \begin{bmatrix}E_{11}/(1-\nu_{21}\nu_{12}) & 0\\ 0 & G_{13}\end{bmatrix}^{(m)}_{(i)}\begin{pmatrix}\varepsilon_x\\ \gamma_{xz}\end{pmatrix}_{(i)},\end{aligned} \tag{2.14}$$

where $\overline{\boldsymbol{C}}^{(m)}_{(i)}$ is the stiffness matrix of the m^{th} layer within the i^{th} ESL. By using the constitutive equations the stress resultants are calculated by integrating the stresses over the thickness of each ESL:

$$\begin{pmatrix}N_x\\ M_x\\ L_x\\ P_x\end{pmatrix}_{(i)} = \int_0^b \int_{-t_i/2}^{t_i/2} \sigma_x \begin{pmatrix}1\\ y\\ y^2\\ y^3\end{pmatrix}_{(i)} dz^{(i)}dy, \tag{2.15}$$

and:

$$\begin{pmatrix}Q_{xz}\\ R_{xz}\\ S_{xz}\end{pmatrix}_{(i)} = \int_0^b \int_{-t_i/2}^{t_i/2} \tau_{xz} \begin{pmatrix}1\\ y\\ y^2\end{pmatrix}_{(i)} dz^{(i)}dy. \tag{2.16}$$

The relationship between the strain field and the stress resultants can be determined by taking back Eqs.(2.14) and (2.15)-(2.16):

$$\begin{pmatrix}N_x\\ M_x\\ L_x\\ P_x\end{pmatrix}_{(i)} = \begin{bmatrix}A_{11} & B_{11} & D_{11} & E_{11}\\ B_{11} & D_{11} & E_{11} & F_{11}\\ D_{11} & E_{11} & F_{11} & G_{11}\\ E_{11} & F_{11} & G_{11} & H_{11}\end{bmatrix}_{(i)}\begin{pmatrix}\varepsilon^{(0)}\\ \varepsilon^{(1)}\\ \varepsilon^{(2)}\\ \varepsilon^{(3)}\end{pmatrix}_{(i)}, \tag{2.17}$$

$$\begin{pmatrix}Q_{xy}\\ R_{xy}\\ S_{xy}\end{pmatrix}_{(i)} = \begin{bmatrix}A_{55} & B_{55} & D_{55}\\ B_{55} & D_{55} & E_{55}\\ D_{55} & E_{55} & F_{55}\end{bmatrix}_{(i)}\begin{pmatrix}\gamma^{(0)}_{xy}\\ \gamma^{(1)}_{xy}\\ \gamma^{(2)}_{xy}\end{pmatrix}_{(i)}, \tag{2.18}$$

where $N_{x(i)}$ denotes the normal force, $M_{x(i)}$ represents the bending moment, $Q_{x(i)}$ is the transverse shear force, and finally $L_{x(i)}$, $P_{x(i)}$, $R_{x(i)}$, $S_{x(i)}$ are the higher-order stress resultants [5]. In Eqs.(2.17)-(2.18) $A_{pp(i)}$ is the extensional, $B_{pp(i)}$ is the coupling, $D_{pp(i)}$ is the bending, $E_{pp(i)}$, $F_{pp(i)}$, $G_{pp(i)}$ and $H_{pp(i)}$ are higher-order stiffnesses defines as:

$$(A_{pp}, B_{pp}, D_{pp}, E_{pp}, F_{pp}, G_{pp}, H_{pp})_{(i)} = \sum_{m=1}^{N_{l(i)}} \int_0^b \int_{y_m^{(i)}}^{y_{m+1}^{(i)}} \overline{C}^{(m)}_{pp}(1, z, z^2, z^3, z^4, z^5, z^6)^{(i)} dz^{(i)}dy, \tag{2.19}$$

where $N_{l(i)}$ is the number of layers within i^{th} ESL [5]. The stiffnesses above have to be calculated with respect to the local reference planes for each ESL. Thus, obtaining:

$$\begin{aligned}
A_{pp(i)} &= b\sum_{m=1}^{N_{l(i)}}\overline{C}_{pp}^{(m)}(z_{m+1}^{(i)}-z_m^{(i)}), & B_{pp(i)} &= b\frac{1}{2}\sum_{m=1}^{N_{l(i)}}\overline{C}_{pp}^{(m)}([z_{m+1}^{(i)}]^2-[z_m^{(i)}]^2),\\
D_{pp(i)} &= b\frac{1}{3}\sum_{m=1}^{N_{l(i)}}\overline{C}_{pp}^{(m)}([z_{m+1}^{(i)}]^3-[z_m^{(i)}]^3), & E_{pp(i)} &= b\frac{1}{4}\sum_{m=1}^{N_{l(i)}}\overline{C}_{pp}^{(m)}([z_{m+1}^{(i)}]^4-[z_m^{(i)}]^4),\\
F_{pp(i)} &= b\frac{1}{5}\sum_{m=1}^{N_{l(i)}}\overline{C}_{pp}^{(m)}([z_{m+1}^{(i)}]^5-[z_m^{(i)}]^5), & G_{pp(i)} &= b\frac{1}{6}\sum_{m=1}^{N_{l(i)}}\overline{C}_{pp}^{(m)}([z_{m+1}^{(i)}]^6-[z_m^{(i)}]^6),\\
H_{pp(i)} &= b\frac{1}{7}\sum_{m=1}^{N_{l(i)}}\overline{C}_{pp}^{(m)}([z_{m+1}^{(i)}]^7-[z_m^{(i)}]^7), & p &= 1 \ or \ 5,
\end{aligned} \quad , \tag{2.20}$$

where b is the beam width, z_m^i and z_{m+1}^i are the local bottom and top coordinates of the m^{th} layer in the i^{th} ESL [1]. By using the stress resultants by Eqs.(2.17)-(2.18) and the virtual strains the virtual strain energy of the i^{th} ESL becomes:

$$\begin{aligned}
\delta U_{(i)} = \int_{(l)} \Big\{ & N_{x(i)}\delta\varepsilon_{x(i)}^{(0)} + M_{x(i)}\delta\varepsilon_{x(i)}^{(1)} + L_{x(i)}\delta\varepsilon_{x(i)}^{(2)} + P_{x(i)}\delta\varepsilon_{x(i)}^{(3)} \\
& + Q_{xz(i)}\delta\gamma_{xz(i)}^{(0)} + R_{xz(i)}\delta\gamma_{xz(i)}^{(1)} + S_{xz(i)}\delta\gamma_{xz(i)}^{(2)} \Big\} dx.
\end{aligned} \tag{2.21}$$

To transform Eq.(2.21) further the chain rule and the divergence theorem can be used [1]:

$$N_x\frac{\partial(\delta u_0)}{\partial x} = \frac{\partial(N_x\delta u_0)}{\partial x} - \frac{N_x}{\partial x}\delta u_0 ..., \int_{(l)}\frac{\partial(N_x\delta u_0)}{\partial x}dl = \oint_{\Gamma_{(l)}} n_x(N_x\delta u_0)ds ..., \ etc. \tag{2.22}$$

Finally, the following can be written:

$$\begin{aligned}
\delta U_{(i)} = & \int_{(l)} \Big\{ - N_{x(i),x}\delta u_0 - N_{x(i),x}K_{ij}^{(0)}\delta\psi_{(x)j} - M_{x(i),x}K_{ij}^{(1)}\delta\psi_{(x)j} \\
& - L_{x(i),x}K_{ij}^{(2)}\delta\psi_{(x)j} - P_{x(i),x}K_{ij}^{(3)}\delta\psi_{(x)j} + Q_{x(i),x}K_{ij}^{(1)}\delta\psi_{(x)j} \\
& + R_{x(i),x}K_{ij}^{(2)}\delta\psi_{(x)j} + S_{x(i),x}K_{ij}^{(3)}\delta\psi_{(x)j} - Q_{x(i),x}\delta v \Big\} dx \\
& + \int_{\Gamma_{(l)}} \Big\{ N_{x(i)}n_{x(i)}\delta u_0 + N_{x(i)}n_{x(i)}K_{ij}^{(0)}\delta\psi_{(x)j} + M_{x(i)}n_{x(i)}K_{ij}^{(1)}\delta\psi_{(x)j} \\
& + L_{x(i)}n_{x(i)}K_{ij}^{(2)}\delta\psi_{(x)j} + P_{x(i)}n_{x(i)}K_{ij}^{(3)}\delta\psi_{(x)j} + Q_{x(i)}n_{x(i)}K_{ij}^{(1)}\delta\psi_{(x)j} \\
& + R_{x(i)}n_{x(i)}K_{ij}^{(2)}\delta\psi_{(x)j} + S_{x(i)}n_{x(i)}K_{ij}^{(3)}\delta\psi_{(x)j} + Q_{x(i)}n_{x(i)}\delta v \Big\} dx,
\end{aligned} \tag{2.23}$$

where the comma means differentiation. The first term in the Eq.(2.23) is the virtual strain energy related to the volume domain of the ESL, the second term represents the boundary conditions. Finally, the virtual work of external forces for a ESL is:

$$\delta W_{F(i)} = \int\limits_{\Omega_0} \left\{ q_{b(i)}(x)\delta w(x, -t_i/2) + q_{t(i)}(x)\delta w(x, t_i/2) \right\} dx, \tag{2.24}$$

where q_b and q_t are the distributed loads on the top and bottom parts of the i^{th} ESL. The equilibrium equations can be obtained by setting the coefficient of virtual displacement parameteres in the virtual work expression Eq.(2.11) using Eqs.(2.23) and (2.24) on the domain l equal to zero. [1, 5]. The equilibrium equations, separately for undelaminated and delaminated portions, are discussed in the further subsections.

2.4 Equilibrium equations - Invariant form

In the sequel the equilibrium equations are detailed separately for the undelaminated and delaminated regions.

2.4.1 Undelaminated region

By setting the sum of coefficients for the virtual membrane displacement δu_0, primary parameters $\delta\psi_j$ and the deflection δw in Eq.(2.11) to zero by using Eqs:(2.23)-(2.24) leads to three types of equilibrium equations. By using normal stress resultants, the form of equilibrium equation becomes absolutely independent of the above mentioned theories (FSDT, SSDT, TSDT). Each and every case it can be written as:

$$\delta u_0 : \sum_{i=1}^{k} \left(\frac{\partial N_{x(i)}}{\partial x} \right) = 0, \tag{2.25}$$

where k is the total number of ESLs. Although, the definition of the normal forces are not independent of the applied theory referring to Eq.(2.17). Generally, using any higher order theory, the number of primary parameters (ignoring the global membrane displacements) in the displacement field is r, which is equal to the number of elements in $\boldsymbol{\psi_p}$. By collecting the coefficients of the virtual primary displacement parameters in Eq.(2.11) and make them equal to zero the following equations can be read out:

$$\begin{aligned} \delta\psi_j : \sum_{i=1}^{k} \Bigg(& K_{ij}^{(0)} \frac{\partial N_{x(i)}}{\partial x} + K_{ij}^{(1)} \frac{\partial M_{x(i)}}{\partial x} + K_{ij}^{(2)} \frac{\partial L_{x(i)}}{\partial x} + K_{ij}^{(3)} \frac{\partial P_{x(i)}}{\partial x} - \\ & K_{ij}^{(1)} Q_{x(i)} - 2K_{ij}^{(2)} R_{x(i)} - 3K_{ij}^{(3)} S_{x(i)} \Bigg) = 0, \end{aligned} \tag{2.26}$$

where ψ_j denotes the primary parameters and $j = 1..q$. Similarly to the normal force equlibrium, by collecting the coefficients of the $\delta w(x)$ beam deflection and setting their sum to zero in Eq.(2.11) leads to:

$$\delta w : \sum_{i=1}^{k} \left(\frac{\partial Q_{x(i)}}{\partial x} \right) + q = 0, \tag{2.27}$$

where q is the external distributed force along the beam:

$$q = \sum_{i=1}^{k} \Big(q_{b(i)} + q_{t(i)} \Big). \tag{2.28}$$

This form is also idependent of the applied theory, although, definition of the shear forces are not, referring to Eq.(2.18).

The previous equations define the invariant form of the equilibrium equations. Using any theory and any number of layers, by calculating K_{ij} displacement multiplicator matrix elements and defining $\boldsymbol{\psi_p}$ vector of primary parameters, the expression of the equilibrium equations is possible to obtain[5].

2.4.2 Delaminated region

The delaminated regions consist of a top and a bottom beam. Each of them is modeled by further ESLs. The most essential difference between the delaminated and undelaminated plate regions is that in the delaminated region the displacements are not connected to each other at the delaminated plane. Therefore, the global membrane displacement u_0 is replaced by u_{0b} for ESLs of the bottom plate, moreover, by u_{0t} for the ESLs of the top plate in Eq.(2.7):

$$\begin{aligned} u_{(i)} &= u_{0b} + \Big(K_{ij}^{(0)} + K_{ij}^{(1)} y^{(i)} + K_{ij}^{(2)} [y^{(i)}]^2 + K_{ij}^{(3)} [y^{(i)}]^3 \Big) \psi_j, \quad i = 1..h, \\ u_{(i)} &= u_{0t} + \Big(K_{ij}^{(0)} + K_{ij}^{(1)} y^{(i)} + K_{ij}^{(2)} [y^{(i)}]^2 + K_{ij}^{(3)} [y^{(i)}]^3 \Big) \psi_j, \quad i = h+1..k, \end{aligned} \tag{2.29}$$

where h is the number of ESLs in the bottom beam and j is a summation index. Furthermore, the w tranverse deflection is also separated into bottom and top deflections:

$$\begin{aligned} w_{(i)} &= w_b, \quad i = 1..h, \\ w_{(i)} &= w_t, \quad i = h+1..k. \end{aligned} \tag{2.30}$$

As a consequence, the equilibrium equations of the normal forces and the transverse forces get separated from each other:

$$\delta u_{0b} : \sum_{i=1}^{h} \left(\frac{\partial N_{x(i)}}{\partial x} \right) = 0, \qquad \delta u_{0t} : \sum_{i=h+1}^{k} \left(\frac{\partial N_{x(i)}}{\partial x} \right) = 0, \tag{2.31}$$

$$\delta w_b : \sum_{i=1}^{h} \left(\frac{\partial Q_{x(i)}}{\partial x} \right) + q_b = 0, \quad \delta w_t : \sum_{i=h+1}^{k} \left(\frac{\partial Q_{x(i)}}{\partial x} \right) + q_t = 0. \tag{2.32}$$

The form of the other equilibrium equations, of course with different K_{ij} displacement multiplicator matrix elements, are formulated according to Eq.(2.26).

Chapter 3

The method of four equivalent single layers

In this chapter the concept of semi-layerwise technique is utilized, separately for the undelaminated and delaminated portions. The whole laminate is modeled by 4ESLs. Two layers of the model are located above and further two below the delamination plane resulting four layers in the undelaminated part [5, 7, 8].

3.1 Undelaminated region

The concept of the method using 4ESLs in the undelaminated portion is illustrated by Figure 3.1. The displacement function is piecewise linear by FSDT, piecewise quadratic in the case of the SSDT and cubic for the TSDT. The corresponding shear strain distributions are shown in 3.1b. It is piecewise constant by FSDT, piecewise linear by SSDT and piecewise quadratic by TSDT with continuous derivatives and curvatures in the interface plane 1-2

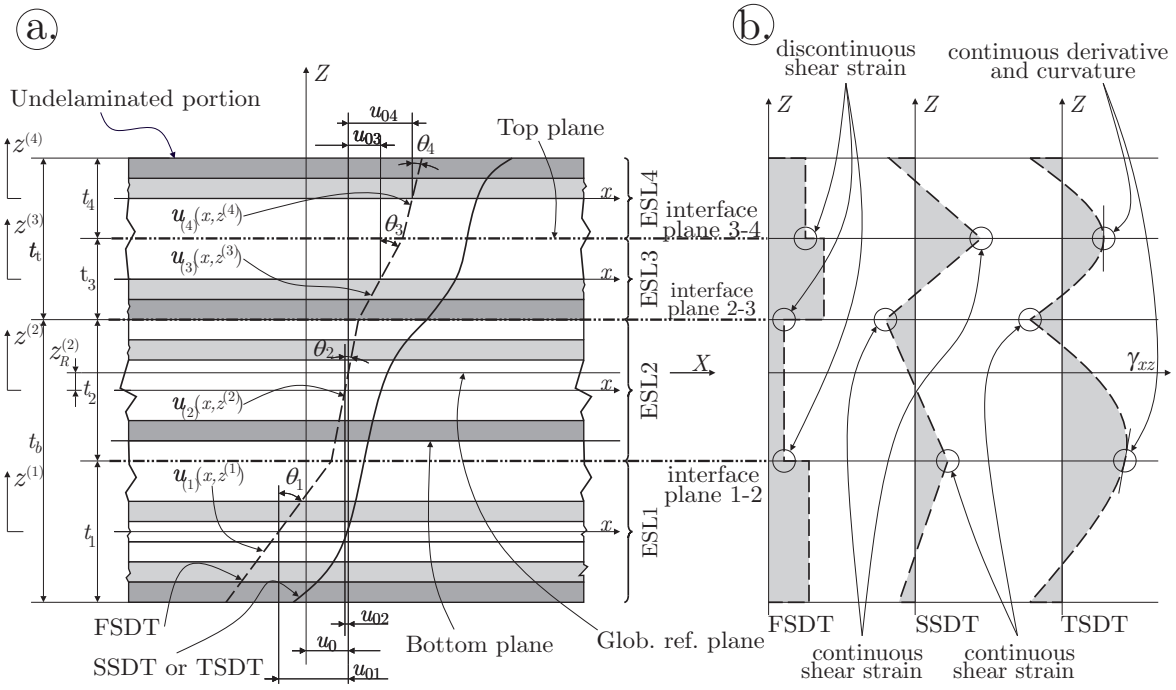

FIGURE 3.1: Cross section and the assumed deformation of the undelaminated portion in the $X - Z$ plane (a) and distributions of the transverse shear strain by different theories (b) using 4ESLs.

and in the interface plane 3-4 [7]. According to the Eqs.(2.2)-(2.6), the following conditions can be formulated between the 4ESLs by starting with the continuity conditions:

$$\begin{aligned}
&(u_{(1)}, w_{(1)})\Big|_{z^{(1)}=t_1/2} = (u_{(2)}, w_{(2)})\Big|_{z^{(2)}=-t_2/2}, \\
&(u_{(2)}, w_{(2)})\Big|_{z^{(2)}=t_2/2} = (u_{(3)}, w_{(3)})\Big|_{z^{(3)}=-t_3/2}, \\
&(u_{(3)}, w_{(3)})\Big|_{z^{(3)}=t_3/2} = (u_{(4)}, w_{(4)})\Big|_{z^{(4)}=-t_4/2}.
\end{aligned} \tag{3.1}$$

The reference plane belongs to the second ESL, therefore, the following condition is imposed referring to Eq.(2.3):

$$u_{(2)}\Big|_{z^{(2)}=z_R^{(2)}} - u_0(x) = 0, \tag{3.2}$$

where $z_R^{(2)} = 1/2(t_3 + t_4 - t_1)$ in accordance with Figure 3.1a and it gives the location of the global midplane of the model with respect to ESL2. The next set of conditions decribes the continuous shear strain at the interface plane using Eq.(2.4):

$$\begin{aligned}
&\gamma_{xz(1)}\Big|_{z^{(1)}=t_1/2} = \gamma_{xz(2)}\Big|_{z^{(2)}=-t_2/2}, \\
&\gamma_{xz(2)}\Big|_{z^{(2)}=t_2/2} = \gamma_{xz(3)}\Big|_{z^{(3)}=-t_3/2}, \\
&\gamma_{xz(3)}\Big|_{z^{(3)}=t_3/2} = \gamma_{xz(4)}\Big|_{z^{(4)}=-t_4/2}.
\end{aligned} \tag{3.3}$$

As it was previously discussed by Eqs.(2.4) and (2.5), the contiuous shear strain derivates and curvatures can be imposed in the case of TSDT at interface planes 1-2 and 3-4:

$$\begin{aligned}
&\frac{\partial \gamma_{xz(1)}}{\partial z^{(1)}}\Big|_{z^{(1)}=t_1/2} = \frac{\partial \gamma_{xz2)}}{\partial z^{(2)}}\Big|_{-z^{(2)}=t_2/2}, \\
&\frac{\partial \gamma_{xz(3)}}{\partial z^{(3)}}\Big|_{z^{(3)}=t_3/2} = \frac{\partial \gamma_{xz(4)}}{\partial z^{(4)}}\Big|_{-z^{(4)}=t_4/2},
\end{aligned} \tag{3.4}$$

and:

$$\begin{aligned}
&\frac{\partial^2 \gamma_{xz(1)}}{\partial \left(z^{(1)}\right)^2}\Big|_{z^{(1)}=t_1/2} = \frac{\partial^2 \gamma_{xz(2)}}{\left(\partial z^{(2)}\right)^2}\Big|_{-z^{(2)}=t_2/2}, \\
&\frac{\partial^2 \gamma_{xz(3)}}{\partial \left(z^{(3)}\right)^2}\Big|_{z^{(3)}=t_3/2} = \frac{\partial^2 \gamma_{xz(4)}}{\left(\partial z^{(4)}\right)^2}\Big|_{-z^{(4)}=t_4/2}.
\end{aligned} \tag{3.5}$$

If the displacement functions are modified in order to satisfy Eqs.(3.1)-(3.5) then, using FSDT, SSDT or TSDT, the displacement functions can be formulated as:

$$\begin{aligned}
&u_{(i)} = u_0 + \left(K_{ij}^{(0)} + K_{ij}^{(1)} z^{(i)} + K_{ij}^{(2)} [z^{(i)}]^2 + K_{ij}^{(3)} [z^{(i)}]^3\right) \psi_j, \quad i = 1..4 \\
&w_{(i)} = w(x), \quad i = 1..4,
\end{aligned} \tag{3.6}$$

where the matrices denoted by K_{ij} are related only to the geometry, i refers to the ESL number, the summation index j defines the component in ψ_j, which is the vector of primary parameters, and finally $w(x)$ is the tranverese deflection identical for each ESL [5].

3.1.1 Third-order beam theory

Using the above mentioned exact kinematic conditions by Eqs.3.1-3.5, 11 unknown displacement parameters can be eliminated from the original 18 parameters. The secondary parameters are: $u_{0(i)}$, $\lambda_{(i)}$ for $i = 1..4$, $\theta_{(i)}$ for $i = 1, 2$ and 4. The unknown terms and the vector of primary parameters are:

$$u_0, \quad w, \quad \boldsymbol{\psi_p} = \begin{pmatrix} \theta_3 & \phi_1 & \phi_2 & \phi_3 & \phi_4 \end{pmatrix}^T. \tag{3.7}$$

The elements of the matrices $K_{ij}^{(0)}$, $K_{ij}^{(1)}$, $K_{ij}^{(2)}$ and $K_{ij}^{(3)}$ in Eq.(3.6) are defined in Appendix A.1. The equilibrium equations can be obtained using Eqs.(2.25)-(2.27) and the vector of primary parameters from Eq.(3.7):

$$\delta u_0 : \sum_{i=1}^{k} \left(\frac{\partial N_{x(i)}}{\partial x} \right) = 0, \tag{3.8}$$

$$\begin{aligned} \delta \psi_j : \sum_{i=1}^{4} \Bigg(& K_{ij}^{(0)} \frac{\partial N_{x(i)}}{\partial x} + K_{ij}^{(1)} \frac{\partial M_{x(i)}}{\partial x} + K_{ij}^{(2)} \frac{\partial L_{x(i)}}{\partial x} + K_{ij}^{(3)} \frac{\partial P_{x(i)}}{\partial x} - \\ & K_{ij}^{(1)} Q_{x(i)} - 2K_{ij}^{(2)} R_{x(i)} - 3K_{ij}^{(3)} S_{x(i)} \Bigg) = 0, \quad j = 1..5, \end{aligned} \tag{3.9}$$

$$\delta w : \sum_{i=1}^{4} \left(\frac{\partial Q_{x(i)}}{\partial x} \right) + q = 0. \tag{3.10}$$

3.1.2 Second-order beam theory

In this case, by using similarly the exact kinematic conditions by Eqs.3.1-3.3, apart from the continuity of derivatives and curvatures, 7 unknown displacement parameters can be eliminated by means of the original 14 parameters. The secondary parameters are: $u_{0(i)}$, $\theta_{(i)}$ for $i = 2, 4$, $\phi_{(i)}$ for $i = 1$ and 3. The unknown terms and the vector of primary parameters are:

$$u_0, \quad w, \quad \boldsymbol{\psi_p} = \begin{pmatrix} \theta_1 & \theta_3 & \phi_1 & \phi_2 & \phi_4 \end{pmatrix}^T. \tag{3.11}$$

Obviously, in this case, $K_{ij}^{(3)} = 0$. The elements of the matrices $K_{ij}^{(0)}$,$K_{ij}^{(1)}$ and $K_{ij}^{(2)}$ in Eq.(3.6) are specified by Appendix A.2. The equilibrium equations take the same form as Eqs.(2.25)-(2.27) and the vector of primary parameters from Eq.(3.11)

3.1.3 First-order beam theory

Apart from the continuity of strains and its derivatives , using similarly the exact kinematic conditions Eqs.3.1-3.2, 4 unknown displacement parameters can be eliminated from the original 10 parameters. These secondary parameters are: $u_{0(i)}$ for $i = 1, 4$. The unknown terms and the vector of primary parameters become:

$$u_0, \qquad w, \qquad \boldsymbol{\psi_p} = \begin{pmatrix} \theta_1 & \theta_2 & \theta_3 & \theta_4 \end{pmatrix}^T \tag{3.12}$$

Obviously, in this case, $K_{ij}^{(3)} = K_{ij}^{(2)} = 0$. The elements of the matrices $K_{ij}^{(0)}$ and$K_{ij}^{(1)}$ in Eq.(3.6) are defined in Appendix A.3. The equilibrium equations take the same form as Eqs.(2.25)-(2.27) associated to the vector of primary parameters from Eq.(3.12).

3.2 Delaminated region

Similarly to the previously introduced kinematic conditions, displacement and strain conditions can be imposed at the interface planes. Although, contrary to the undelaminated case, in the delaminated region the top adn bottom beams are equally modelled by 2-2ESLs. Apart from the delaminated plane, the adjacent layers are connected to each other. Thus, the delaminated regions are described by separated mathematical functions, as it is illustrated by Figure 3.2. As it is depicted in the figure, continuity conditions can be written in the

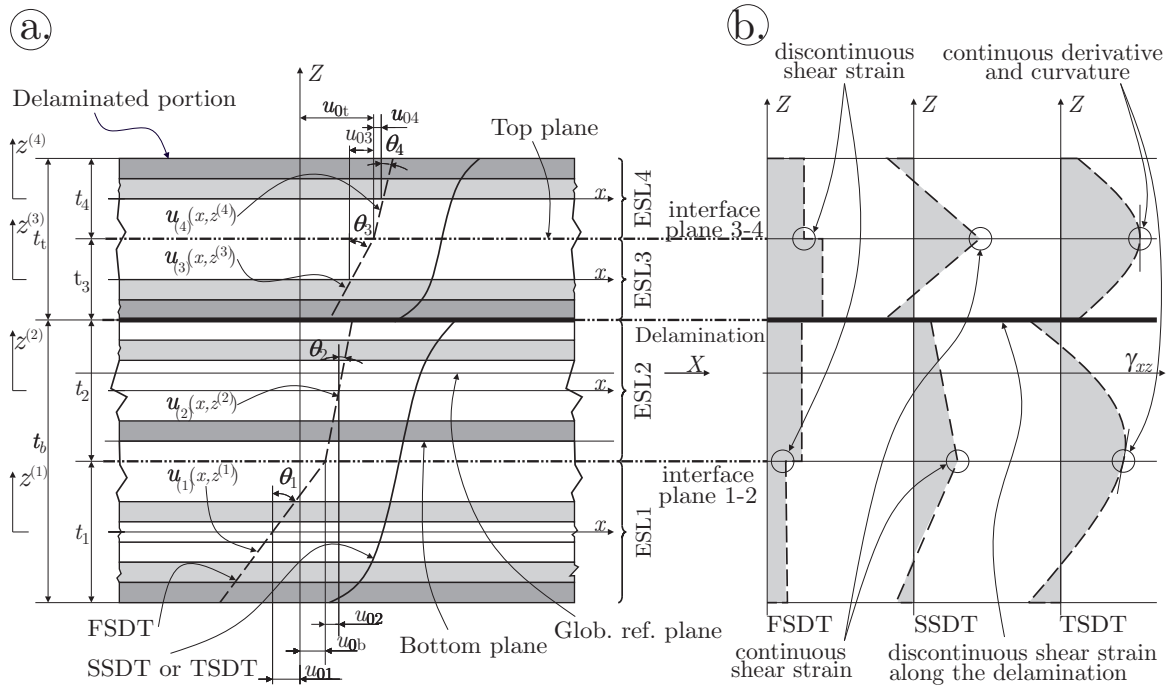

FIGURE 3.2: The assumed deformation of the delaminated portion in the $X - Z$ plane (a) and distributions of the transverse shear strain by different theories (b) using separately 2ESLs.

interface planes 1-2 and 3-4:

$$\begin{aligned}(u_{(1)}, w_{(1)})\Big|_{z^{(1)}=t_1/2} &= (u_{(2)}, w_{(2)})\Big|_{z^{(2)}=-t_2/2},\\ (u_{(3)}, w_{(3)})\Big|_{z^{(3)}=t_3/2} &= (u_{(4)}, w_{(4)})\Big|_{z^{(4)}=-t_4/2}.\end{aligned} \tag{3.13}$$

The reference planes belong to the first and third ESLs:

$$\begin{aligned}u_{(1)}\Big|_{z^{(1)}} &= t_2/2 - u_{0b}(x) = 0,\\ u_{(3)}\Big|_{z^{(3)}} &= t_4/2 - u_{0t}(x) = 0,\end{aligned} \tag{3.14}$$

where u_{0b} and u_{0t} are the global membrane displacements of the bottom and top sublaminates in accordance with Figure 3.2a. In the case of SSDT and TSDT, apart from the delaminated plane, shear strain continuities can be imposed also:

$$\begin{aligned}\gamma_{xz(1)}\Big|_{z^{(1)}=t_1/2} &= \gamma_{xz(2)}\Big|_{z^{(2)}=-t_2/2},\\ \gamma_{xz(3)}\Big|_{z^{(3)}=t_3/2} &= \gamma_{xz(4)}\Big|_{z^{(4)}=-t_4/2}.\end{aligned} \tag{3.15}$$

Furthermore, using TSDT, continuity of the shear strain derivatives is imposed, as well:

$$\begin{aligned}\frac{\partial\gamma_{xz(1)}}{\partial z^{(1)}}\Big|_{z^{(1)}=t_1/2} &= \frac{\partial\gamma_{xz(2)}}{\partial z^{(2)}}\Big|_{-z^{(2)}=t_2/2},\\ \frac{\partial\gamma_{xz(3)}}{\partial z^{(3)}}\Big|_{z^{(3)}=t_3/2} &= \frac{\partial\gamma_{xz(4)}}{\partial z^{(4)}}\Big|_{-z^{(4)}=t_4/2},\end{aligned} \tag{3.16}$$

and finally, continuity of the shear strain curvatures is ensured by:

$$\begin{aligned}\frac{\partial^2\gamma_{xz(1)}}{\partial\left(z^{(1)}\right)^2}\Big|_{z^{(1)}=t_1/2} &= \frac{\partial^2\gamma_{xz(2)}}{\left(\partial z^{(2)}\right)^2}\Big|_{-z^{(2)}=t_2/2},\\ \frac{\partial^2\gamma_{xz(3)}}{\partial\left(z^{(3)}\right)^2}\Big|_{z^{(3)}=t_3/2} &= \frac{\partial^2\gamma_{xz(4)}}{\left(\partial z^{(4)}\right)^2}\Big|_{-z^{(4)}=t_4/2}.\end{aligned} \tag{3.17}$$

The displacement functions are given by the following equations:

$$\begin{aligned}u_{(i)} &= u_{0b} + \left(K_{ij}^{(0)} + K_{ij}^{(1)} z^{(i)} + K_{ij}^{(2)}[z^{(i)}]^2 + K_{ij}^{(3)}[z^{(i)}]^3\right)\psi_j, \quad i = 1..2,\\ u_{(i)} &= u_{0t} + \left(K_{ij}^{(0)} + K_{ij}^{(1)} z^{(i)} + K_{ij}^{(2)}[z^{(i)}]^2 + K_{ij}^{(3)}[z^{(i)}]^3\right)\psi_j, \quad i = 3..4,\\ w_{(i)} &= w_b(x), \quad i = 1..2,\\ w_{(i)} &= w_t(x), \quad i = 3..4,\end{aligned} \tag{3.18}$$

where notations, apart from the transverse deflections, are exactly the same as given by Eq.(3.6). Moreover, w_b denotes the tranverse deflection of the bottom beam and w_t represents deflection of the top beam.

3.2.1 Third-order beam theory

Utilizing the above mentioned exact kinematic conditions by Eqs.(3.13)-(3.17), 10 unknown displacement parameters can be eliminated from the 20 parameters. The secondary parameters are: $u_{0(i)}$, $\lambda_{(i)}$ for $i = 1..4$, $\theta_{(i)}$ for $i = 2$ and 4. Thus the unknown terms and the vector of primary parameters are:

$$u_{0b}, \quad u_{0t}, \quad w_b, \quad w_t, \quad \boldsymbol{\psi_p} = \begin{pmatrix} \textcircled{θ_1} & \phi_1 & \phi_2 & \theta_3 & \phi_3 & \phi_4 \end{pmatrix}^T, \tag{3.19}$$

where circle denotes the autocontinuity parameter. The role of this term will be discussed later. The elements of the matrices $K_{ij}^{(0)}$, $K_{ij}^{(1)}$, $K_{ij}^{(2)}$ and $K_{ij}^{(3)}$ in Eq.(3.18) are defined in Appendix A.1. The equilibrium equations can be obtained using the previously defined invariant forms by Eqs.(2.25)-(2.27) and the vector of primary parameters from Eq.(3.19):

$$\delta u_{0b} : \sum_{i=1}^{2} \left(\frac{\partial N_{x(i)}}{\partial x} \right) = 0, \quad \delta u_{0t} : \sum_{i=3}^{4} \left(\frac{\partial N_{x(i)}}{\partial x} \right) = 0, \tag{3.20}$$

$$\begin{aligned} \delta \psi_j : \sum_{i=1}^{4} \Bigg(& K_{ij}^{(0)} \frac{\partial N_{x(i)}}{\partial x} + K_{ij}^{(1)} \frac{\partial M_{x(i)}}{\partial x} + K_{ij}^{(2)} \frac{\partial L_{x(i)}}{\partial x} + K_{ij}^{(3)} \frac{\partial P_{x(i)}}{\partial x} - \\ & K_{ij}^{(1)} Q_{x(i)} - 2K_{ij}^{(2)} R_{x(i)} - 3K_{ij}^{(3)} S_{x(i)} \Bigg) = 0, \quad j = 1..6, \end{aligned} \tag{3.21}$$

$$\delta v_b : \sum_{i=1}^{2} \left(\frac{\partial Q_{x(i)}}{\partial x} \right) + q = 0, \quad \delta v_t : \sum_{i=3}^{4} \left(\frac{\partial Q_{x(i)}}{\partial x} \right) + q = 0. \tag{3.22}$$

3.2.2 Second-order beam theory

In the case of SSDT, using Eqs.3.13-3.15, 6 unknown displacement parameters can be eliminated from the original 14 unknown parameters. The secondary parameters are: $u_{0(i)}$ for $i = 1..4$, $\theta_{(i)}$ for $i = 2$ and 4 . The unknown terms and the vector of primary parameters are:

$$u_{0b}, \quad u_{0t}, \quad w_b, \quad w_t, \quad \boldsymbol{\psi_p} = \begin{pmatrix} \theta_1 & \phi_1 & \phi_2 & \theta_3 & \textcircled{ϕ_3} & \phi_4 \end{pmatrix}^T \tag{3.23}$$

Obviously, in this case also, $K_{ij}^{(3)} = 0$. The elements of the matrices $K_{ij}^{(0)}$,$K_{ij}^{(1)}$ and $K_{ij}^{(2)}$ in Eq.3.18 are given in Appendix A.2. The equilibrium equations take the same form as Eqs.(2.25)-(2.27) according to the vector of primary parameters from Eq.(3.23)

3.2.3 First-order beam theory

In this case, using similarly the exact kinematic conditions by Eqs.3.13-3.14, 4 displacement parameters can be eliminated from the original 12 unknown parameters. These secondary parameters are: $u_{0(i)}$ for $i = 1,4$. The unknown terms and the vector of primary parameters are:

$$u_{0b}, \quad u_{0t}, \quad w_b, \quad w_t, \quad \boldsymbol{\psi_p} = \begin{pmatrix} \theta_1 & \theta_2 & \theta_3 & \theta_4 \end{pmatrix}^T \tag{3.24}$$

Obviously, by using FSDT, $K_{ij}^{(3)} = K_{ij}^{(2)} = 0$. The elements of the matrices $K_{ij}^{(0)}$ and $K_{ij}^{(1)}$ in Eq(3.18) are given in Appendix A.3. The equilibrium equations take the same form as Eqs.(2.25)-(2.27) associated to the vector of primary parameters from Eq.(3.24).

Chapter 4

Built-in configuration

In this chapter the previously introduced method of 4ESLs is used to describe the displacement and stress fields around the crack tip in delaminated orthotropic composite beams with built-in end. The different delamination scenarios are pedicted by Figure 4.1. The beams are made from carbon/epoxy material. The material properties (moduli and Poisson's ratios) of the individual laminae are given by Table 4.1 [5]. A single layer is 0.5 mm thick. The lay-up of the undelaminated part is $[\pm 45^f/0/\pm 45_2^f/\bar{0}]_s$ The computations were performed in the code MAPLE. The results are compared to finite element analisys (FEA) where simple 2D PLANE elements were used under plane stress conditions, according to the Figure 1.5.

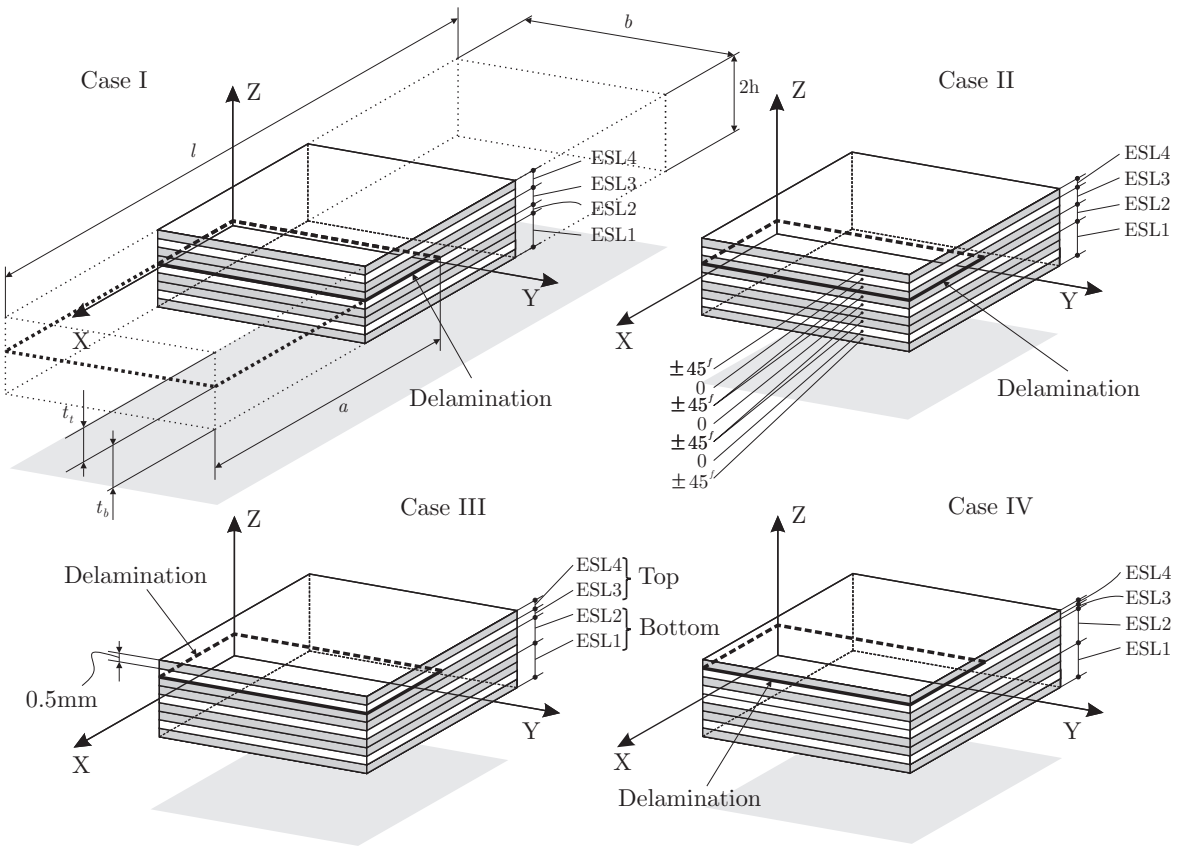

FIGURE 4.1: Different delamination scenarios of a beam element.

	E_{11} [GPa]	E_{22} [GPa]	E_{33} [GPa]	G_{23} [GPa]	G_{13} [GPa]	G_{12} [GPa]	ν_{23} [-]	ν_{13} [-]	ν_{12} [-]
0	148	9.65	9.65	4.91	4.66	3.71	0.27	0.25	0.25
$\pm 45^f$	16.39	16.39	16.4	5.46	5.46	16.4	0.5	0.5	0.3

TABLE 4.1: Elastic properties of single carbon/epoxy composite laminates

4.1 Analytical solution

The geometry of the problem with the associated structure of ESLs is depicted in Figure 4.2, where l is total length, b denotes the width and $2h$ represents the total thickness of the beam. As the delamination splits the structure into a top and bottom sub-laminates, the corresponding thicknesses of these parts are denoted by t_t and t_b. As it was discussed previously, these portions are modelled further with 2-2 ESLs, respectively, resulting 4ESLs in the undelaminated portion. The structure and the thicknesses of the ELSs are determined according to the Figure 4.1.

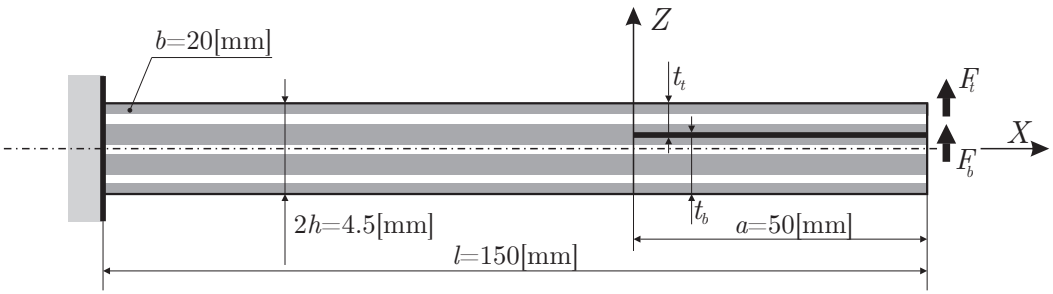

FIGURE 4.2: Built-in configuration of delaminated beam with orthotropic plies.

To perform the analysis, first of all, the necessary continuity and boundary conditions have to be discussed.

4.1.1 Continuity conditions

In the sequel the continuity of displacements and stress resultants between the delaminated and undelaminated regions is detailed. The conditions are imposed against the primary parameters of both regions. The continuity of the membrane displacement components between the top parts of the delaminated and undelaminated regions can be ensured by imposing the equality between the membrane displacements terms on a single ESL in the delaminated part and a single one in the undelaminated one. This statement is also true for the bottom parts, as well. These conditions are satisfied through the following equations:

$$\left(u_0 + \sum_{j=1}^{q_{undel}} K_{1j}^{(0)} \psi_j \Big|_{x=-0}^{(undel)}\right) = \left(u_{0b} + \sum_{j=1}^{q_{del}} K_{1j}^{(0)} \psi_j\right)\Big|_{x=+0}^{(del)}, \tag{4.1}$$

$$\left(u_0 + \sum_{j=1}^{q_{undel}} K_{3j}^{(0)} \psi_j \Big|_{x=-0}^{(undel)}\right) = \left(u_{0t} + \sum_{j=1}^{q_{del}} K_{3j}^{(0)} \psi_j\right)\Big|_{x=+0}^{(del)}, \tag{4.2}$$

meaning two conditions for each theory. The continuity of the deflections involves similarly two conditions:

$$w\Big|_{x=-0}^{(undel)} = w_b\Big|_{x=+0}^{(del)}, \tag{4.3}$$

and

$$w\Big|_{x=-0}^{(undel)} = w_t\Big|_{x=+0}^{(del)}. \tag{4.4}$$

The total continuity of the first-, second-, and third-order terms in the displacement functions can be imposed through the vector of primary paremeters by connecting the first-order terms with first-order terms, the second- and the third-order terms with the corresponding second- and third-order terms. For the TSDT theory, by referring to Eq.(3.7) and (3.19), it can be expressed in the following way:

$$\Big(\theta_3 \quad \psi_1 \quad \psi_2 \quad \psi_2 \quad \psi_4\Big)\Big|_{x=-0}^{(undel)} = \Big(\theta_3 \quad \psi_1 \quad \psi_2 \quad \psi_2 \quad \psi_4\Big)\Big|_{x=+0}^{(del)}, \tag{4.5}$$

meaning q_{undel} number of conditions between the portions. Unfortunately, the number of parameters in the $\boldsymbol{\psi_p}$ vector for the undelaminated and delaminated parts are not equal to each other $q_{del} \neq q_{undel}$. The continuity of these terms cannot be expressed in a simple way beacuse $q_{del} > q_{undel}$. To handle this issue the theorem of auto-continuity has to be applied [8]. The remaining θ_1 term in the primary parameter vector of the delaminated part can be called as auto-continuity parameter, because continuity of this term can be ensured automatically by using only the primary parameters of the undelaminated parts:

$$\begin{aligned}\theta_1\Big|_{x=+0}^{(del)} &= \sum_{j=1}^{q_{undel}} K_{1j}^{(1)}\psi_j\Big|_{x=-0}^{(undel)} \\ &= \Big(\theta_3 - \frac{t_1(t_1+2t_2)\phi_1 + (t_1+2t_2)^2\phi_2}{2(t_1+t_2)} - \frac{(3t_3+2t_4)t_3\phi_3 - t_3^2\phi_4}{2(t_3+t_4)}\Big)\Big|_{x=-0}^{(undel)}.\end{aligned} \tag{4.6}$$

Thus the final number of conditions becomes $q_{undel} + 1 = 5 + 1 = 6$ for TSDT theory. The situation for SSDT theory, by referring to Eq.(3.11) and (3.23), is absolutely the same. The $q_{del} \neq q_{undel}$ inequality can be handled through the following way:

$$\Big(\theta_1 \quad \theta_3 \quad \psi_1 \quad \psi_2 \quad \psi_4\Big)\Big|_{x=-0}^{(undel)} = \Big(\theta_1 \quad \theta_3 \quad \psi_1 \quad \psi_2 \quad \psi_4\Big)\Big|_{x=+0}^{(del)}, \tag{4.7}$$

meaning q_{undel} number of conditions again. The auto-continuity of the remaining ψ_3 in the primary parameter vector of the delaminated part can be ensured by:

$$\phi_3\Big|_{x=+0}^{(del)} = \sum_{j=1}^{q_{undel}} K_{3j}^{(2)}\psi_j\Big|_{x=-0}^{(undel)} = \Big(\frac{-\theta_1 + \theta_3 - t_1\phi_1 - 2t_2\phi_2}{t_3}\Big)\Big|_{x=-0}^{(undel)}. \tag{4.8}$$

Thus the final number of conditions becomes $q_{undel} + 1 = 5 + 1 = 6$ for SSDT theory, as well. Fortunately, in the case of FSDT theory, by referring to Eq.(3.12) and (3.24), the number of parameters in primary parameter vector for undelaminated and delaminated portions are

equal to each other $q_{del} = q_{undel}$. Thus, futher auto-continuity condition is not required to impose the displacement continuity. It can be expressed easily by imposing:

$$\begin{pmatrix} \theta_1 & \theta_2 & \theta_3 & \theta_4 \end{pmatrix}\Big|_{x=-0}^{(undel)} = \begin{pmatrix} \theta_1 & \theta_2 & \theta_3 & \theta_4 \end{pmatrix}\Big|_{x=+0}^{(del)}, \tag{4.9}$$

meaning $q_{del} = q_{undel} = 4$ conditions.

The continuity conditions of stress resultants between the delaminated and undelaminated regions can be imposed by using the equivalent stress resultants [5]. These equations can be directly read out from the equilibrium equations, referring to Eqs.(3.8)-(3.10) and Eqs.(3.20)-(3.22), by omitting derivatives with respect to the x coordinate. In the case of those equlilibrium equations, which correspond to the $\boldsymbol{\psi_p}$ primary parameter vector the $Q_{x(i)}$ shear and the $R_{x(i)}$, $S_{x(i)}$ higher-order shear forces must be omitted also to obtain the equivalent bending moments [1, 5]. According to the Figure 4.3, as a result of arbitrary external forces, $Q_{x(i)}$, $R_{x(i)}$, $S_{x(i)}$ $N_{x(i)}$, $M_{x(i)}$, $L_{x(i)}$ and $P_{x(i)}$ unknown stress resultants are taking place at the end of the delaminated portion in each ESL. These are transferred between the portions in such a way to cause equivalent normal force, equivalent shear force and equivalent bending moments in the undelaminated portion at the delamination front. For the sake of simplicity and because there is not any conventional system in the actual literature to indicate higher-order stress resultants, the same arrows are used to sign them [1] in the above mentioned figure.Therefore, the following equation can be formulated to express the

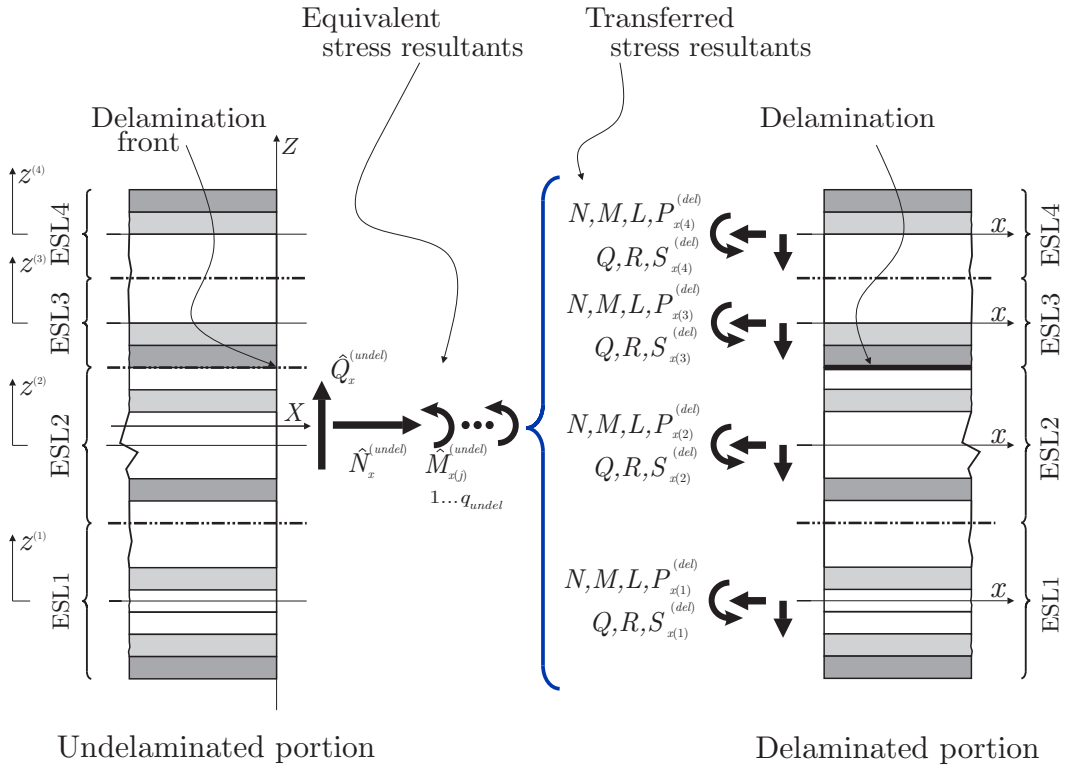

FIGURE 4.3: Continuity of the stress resultants at the delamination front.

continuity of the normal forces at the cross section of delamination tip:

$$\hat{N}_x^{(undel)} = \sum_{i=1}^{4} \left(N_{x(i)} \right) \Big|_{x=-0}^{(undel)} = \sum_{i=1}^{2} \left(N_{x(i)} \right) \Big|_{x=+0}^{(del)} + \sum_{i=3}^{4} \left(N_{x(i)} \right) \Big|_{x=+0}^{(del)}, \tag{4.10}$$

where $\hat{N}_x^{(undel)}$ denotes the equivalent normal force meaning one condition for each theory. The shear force continuity can be described similarly as:

$$\hat{Q}_x^{(undel)} = \sum_{i=1}^{4} \left(Q_{x(i)} \right) \Big|_{x=-0}^{(undel)} = \sum_{i=1}^{2} \left(Q_{x(i)} \right) \Big|_{x=+0}^{(del)} + \sum_{i=3}^{4} \left(Q_{x(i)} \right) \Big|_{x=+0}^{(del)}, \tag{4.11}$$

where $\hat{Q}_x^{(undel)}$ is the equivalent shear force representing a further condition for each case. The final conditions between the portions are the continuity of the equivalent bending moments. These continuity conditions can be formulated as:

$$\begin{aligned} \hat{M}_{x(j)}^{(undel)} &= \sum_{i=1}^{4} \left(K_{ij}^{(0)} \; K_{ij}^{(1)} \; K_{ij}^{(2)} \; K_{ij}^{(3)} \right) \Big|^{(undel)} \cdot \begin{pmatrix} N_{x(i)} \\ M_{x(i)} \\ L_{x(i)} \\ P_{x(i)} \end{pmatrix} \Bigg|_{x=-0}^{(undel)} = \\ &= \sum_{i=1}^{4} \left(K_{ij}^{(0)} \; K_{ij}^{(1)} \; K_{ij}^{(2)} \; K_{ij}^{(3)} \right) \Big|^{(undel)} \cdot \begin{pmatrix} N_{x(i)} \\ M_{x(i)} \\ L_{x(i)} \\ P_{x(i)} \end{pmatrix} \Bigg|_{x=+0}^{(del)}, \qquad j = 1..q_{undel}, \end{aligned} \tag{4.12}$$

where $\hat{M}_{x(j)}^{(undel)}$ denotes the equivalent bending moments imposing four conditions for the FSDT theory and five conditions for the SSDT and TSDT theories.

4.1.2 Boundary conditions

In the case of built-in end, as it is illustrated by Figure 4.2, the displacement field must be zero. Meaning there is no deflection, membrane displacement or even rotation. This condition can be easily imposed be using the primary parameters:

$$u_0 \big|_{x=-l+a}^{(undel)} = 0, \qquad w \Big|_{x=-l+a}^{(undel)} = 0, \qquad \boldsymbol{\psi_p} \Big|_{x=-l+a}^{(undel)} = \mathbf{0}. \tag{4.13}$$

The external forces and bending moments can be taken into account in such a way as the stress resultants are treated in the case of continuity. These similarly cause equivalent shear forces, normal forces and bending moments in the delaminated region, separately for the top and bottom parts. Because there are not any normal forces at the end of the beam, the

following two boundary conitions can be imposed for each theory:

$$\sum_{i=1}^{2}\left(N_{x(i)}\right)\Big|_{x=a}^{(del)}=0, \qquad \sum_{i=3}^{4}\left(N_{x(i)}\right)\Big|_{x=a}^{(del)}=0. \tag{4.14}$$

As it is shown by Figure 4.2, the top and bottom parts of the delaminated regions are loaded with F_t and F_b forces, causing two conditions for each theory:

$$\sum_{i=1}^{2}\left(Q_{x(i)}\right)\Big|_{x=a}^{(del)}=F_t, \qquad \sum_{i=3}^{4}\left(Q_{x(i)}\right)\Big|_{x=a}^{(del)}=F_b. \tag{4.15}$$

And finally, because the lack of any external bending moments:

$$\sum_{i=1}^{4}\left(K_{ij}^{(0)}\ K_{ij}^{(1)}\ K_{ij}^{(2)}\ K_{ij}^{(3)}\right)\Big|^{(del)}\cdot\left(\begin{array}{c}N_{x(i)}\\M_{x(i)}\\L_{x(i)}\\P_{x(i)}\end{array}\right)\Big|_{x=-a}^{(del)}=\left(\begin{array}{c}0\\0\\0\\0\end{array}\right) \qquad j=1..q_{del}, \tag{4.16}$$

representing five boundary conditions for FSDT and six-six conditions for SSDT and TSDT. The applied theories with the number of unknown functions and differential equations are summarized by Table 4.2. This table contains the number of conditions coming from the continuity and the boundary conditions, also.

	FSDT	SSDT	TSDT
No. of Unknown functions	6+8	7+10	7+10
No. of Differential equations	6+8	7+10	7+10
No. of Boundary conditions	(28)	(34)	(34)
Membrane disp. cont. $(x=0)$	1+1	1+1	1+1
Deflection cont. $(x=0)$	1+1	1+1	1+1
Vector of primary par. cont. $(x=0)$	4	5	5
Auto cont. $(x=0)$	0	(+1)	(+1)
Normal force cont. $(x=0)$	1	1	1
Shear force cont. $(x=0)$	1	1	1
Equivalent bending moment cont. $(x=0)$	4	5	5
Built-in end $(x=-l+a)$	2+4	2+5	2+5
Acting normal forces $(x=a)$	1+1	1+1	1+1
Acting shear forces $(x=a)$	1+1	1+1	1+1
Acting equivalent bending moments $(x=a)$	2+2	3+3	3+3
Σ	(28)	(34)	(34)

TABLE 4.2: Summary of the necasary continuity and boundary conditions for each shear deformable theory.

4.2 FEA solution

In order to verify the analytical results finite element (FE) analyses were carried out. The structure of the mesh with the necessary boundary conditions and the applied Davidson mesh to determine energy release rates are depicted in Figure 4.4. The material properties are given by Table 4.1.

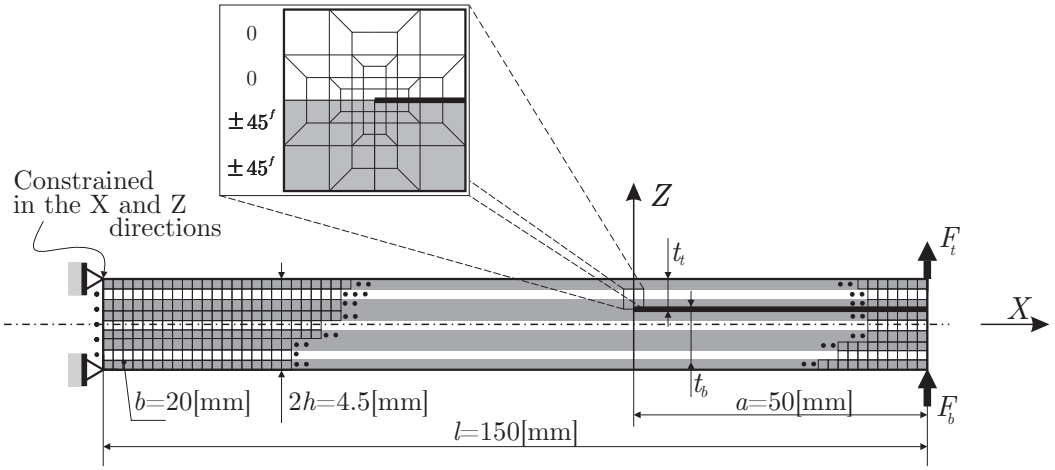

FIGURE 4.4: Discretization of the delaminated beam with the applied Davidson mesh at the crack tip.

4.3 Results - Displacement and stress

In this section the analytical and numerical results are provided in the case of built-in configuration, depicted by Figure 4.2, at the delamination front. The analyses are carried out by using the novel TSDT, SSDT and FSDT solutions. The corresponding dipslacement fields and stress fields are investigated and compared to each other. The actual geometry and the structure of the layers are always indicated in the subsequent figures.

In the case of "Case I" delamination scenario the displacement field is depicted in Figure 4.5. The end of the delaminated sub-laminates are subjected to $F_t = 10$ N and $F_b = -10$ N forces. The u in-plane displacement, using any kind of higher-order theories, agrees very well with the numerical solution. In terms of the w deflections the agreement between numerical and analytical results is also very good. As it was expected, because of the equal and opposite loadings, the delamination opening takes place. Although, the usage of higher-order theories result in a bit smaller values comparing to the numerical set of points, which are determined along the middle lines of the top and bottom parts of the beam. As it is illustrated also in the higlighted part of the figure, the additional contribution of the higher-order theories to the deflection becomes smaller and smaller. Thus, the deflection improvement of the SSDT and TSDT compared with the FSDT is negligible. Using only FSDT the deflection can be obtained with sufficient accuracy.

In order to understand the importance of the higher order theories Figure 4.6 depicts further results in terms of the normal and shear stresses. The stresses are evaluated in the cross section of the delamination tip, respectively, at the undelaminated $X = +0$ [mm] and delaminated $X = -0$ [mm] parts, as well. As a reminder, referring to the Table 4.2, only the continuity conditions of the displacement field can be imposed between the portions resulting certain stress discontinuities at the crack tip. This property of the stress field is highlihted

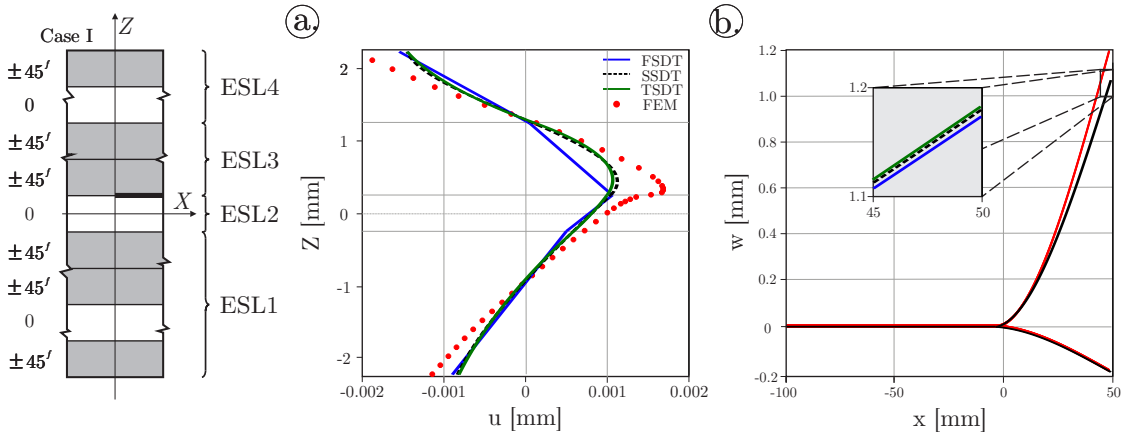

FIGURE 4.5: Distribution of the u displacement at the delamination front (a) and comparison of the deflection along the beam (b), "Case I", F_t = 10 N and F_b = -10 N.

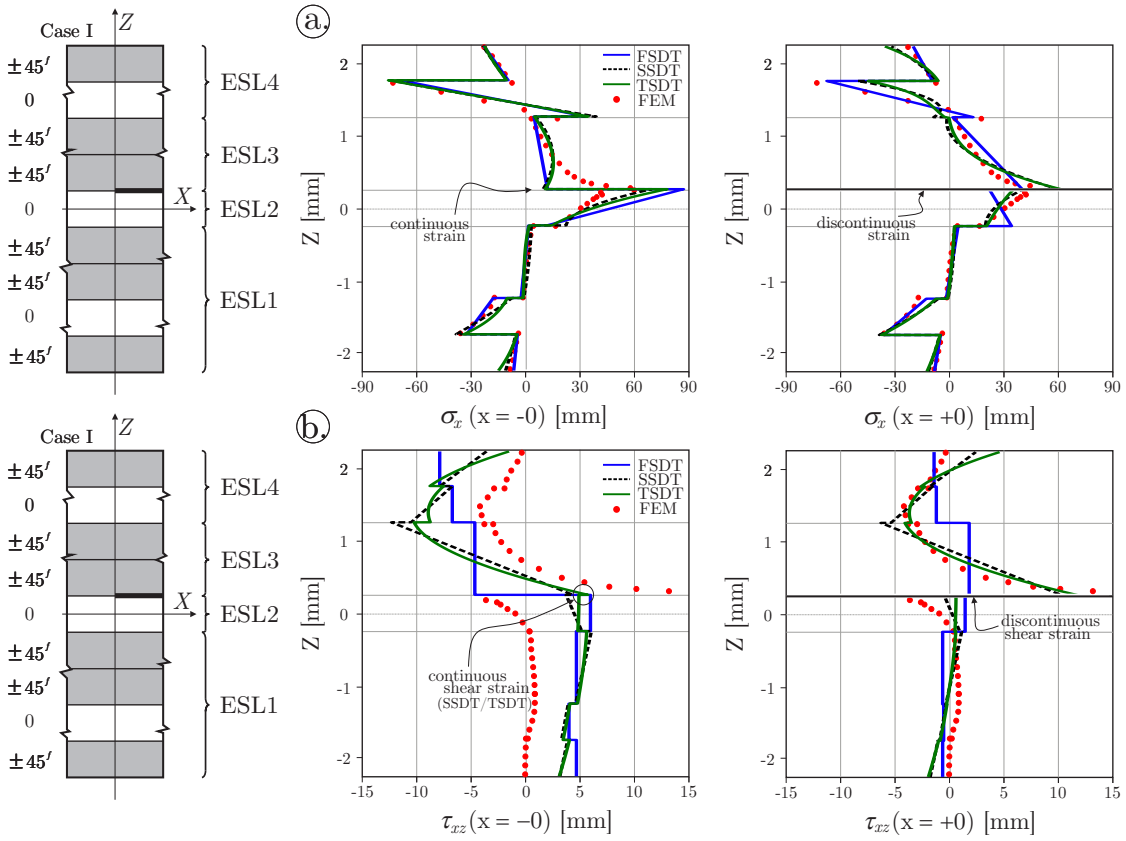

FIGURE 4.6: Distribution of the σ_x normal stresses (a) and the τ_{xz} shear stresses at the delamination tip, "Case I", F_t = 10 N and F_b = -10 N.

in Figure 4.6. As it is shown, in the case of σ_x normal stresses, a quite good agreement with the FEA result can be seen. On the contrary of the analytical solutions, the numerical solution has singular nature in terms of the stress field. Meaning, by decreasing the mesh size around the crack tip the stresses become inevitably higher and higher. Apart from this phenomena, by using reasonable mesh size, the trends of the normal stress solutions are exactly the same, meaning each theory is applicable. Although, in the case of τ_{xz} shear stresses the

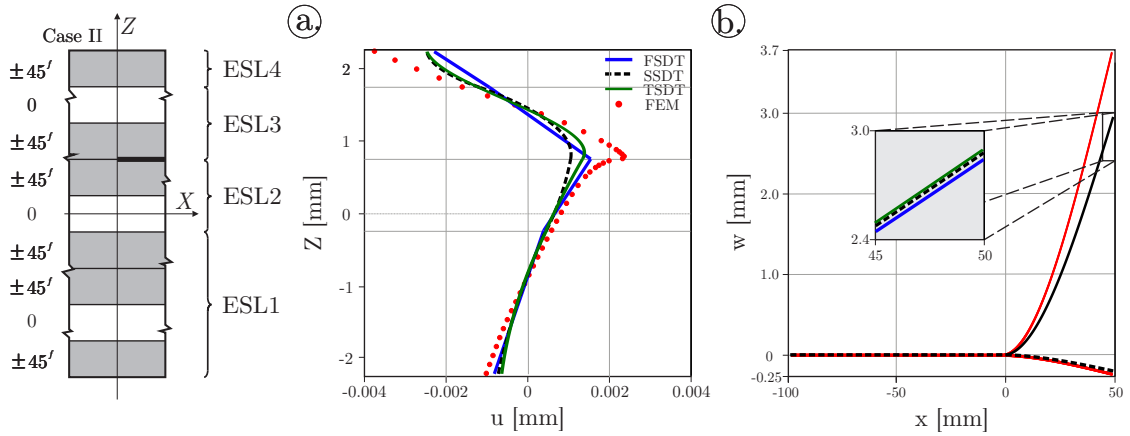

FIGURE 4.7: Distribution of the u displacement at the delamination front (a) and comparison of the deflection along the beam (b), "Case II", $F_t = 10$ N and $F_b =$ -10 N.

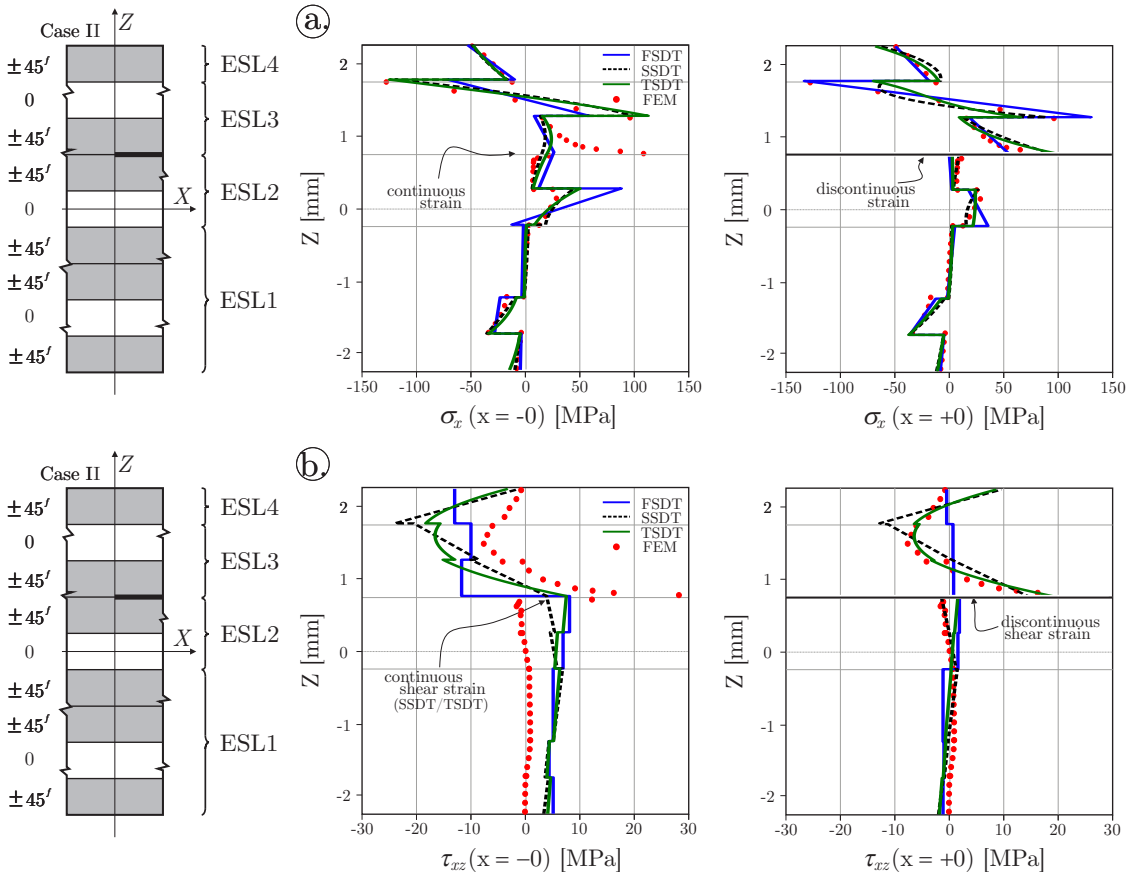

FIGURE 4.8: Distribution of the σ_x normal stresses (a) and the τ_{xz} shear stresses at the delamination tip, "Case II", $F_t = 10$ N and $F_b =$ -10 N.

situation is quite defferent. This is the point where the application of higher-order beam theories makes sense and becomes quite important and significant. According to Figure 4.6b, by increasing the order of solutions, the shear stress can be described with more and more precise way. If the accurate desription of the shear stress is important at the crack tip then the application of higher order theories becomes inevitable.

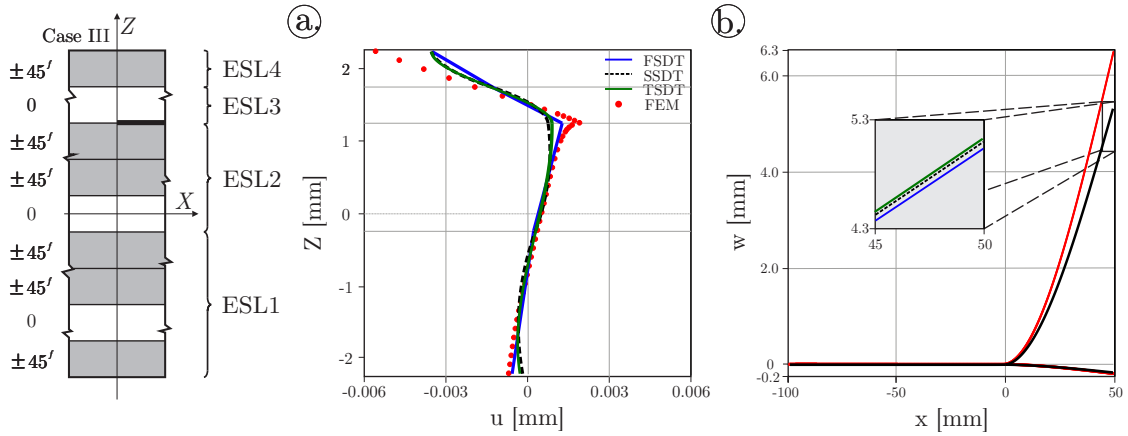

FIGURE 4.9: Distribution of the u displacement at the delamination front (a) and comparison of the deflection along the beam (b), "Case III", $F_t = 10$ N and $F_b =$ -10 N.

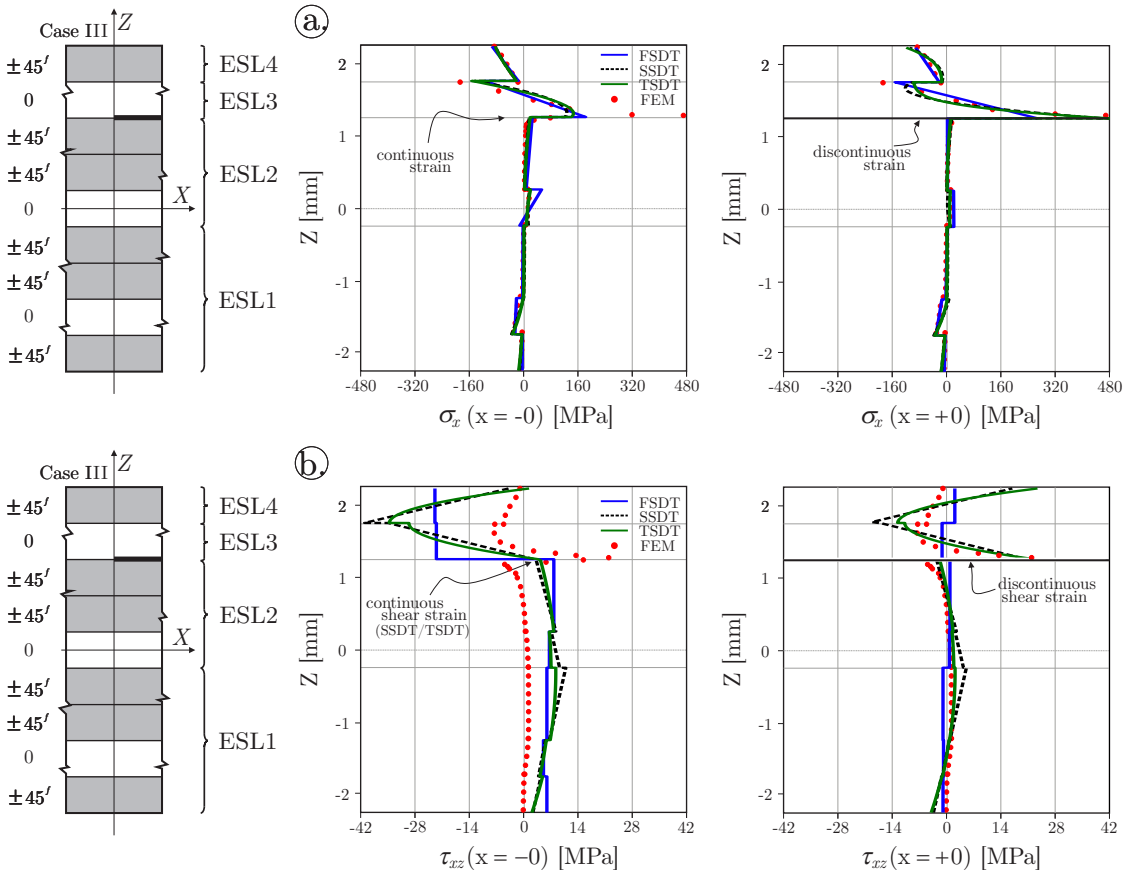

FIGURE 4.10: Distribution of the σ_x normal stresses (a) and the τ_{xz} shear stresses at the delamination tip, "Case III", $F_t = 10$ N and $F_b =$ -10 N.

Similarly to the previous example, "Case II" configuration is loaded with $F_t = 10$ N and $F_b = -10$ N forces. The displacement and stress fields of the delaminated beam are illustrated by Figure 4.7 and 4.8. As it was expected, beacuse the delamination is actually located above its previous location (referring to the "Case I" example), opening of the top sub-laminate is much bigger than the opening of the bottom sub-laminate. In terms of the u

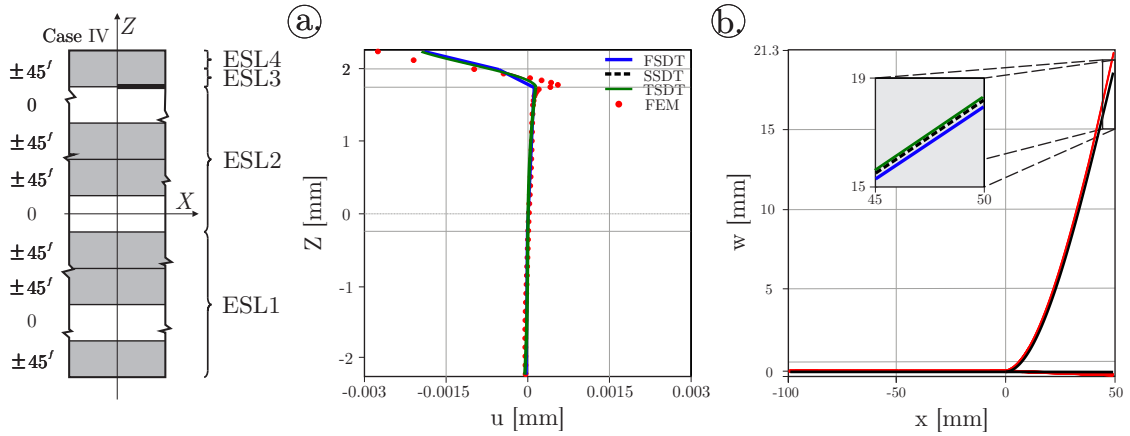

FIGURE 4.11: Distribution of the u displacement at the delamination front (a) and comparison of the deflection along the beam (b), "Case IV", $F_t = 2$ N and $F_b =$ -2 N.

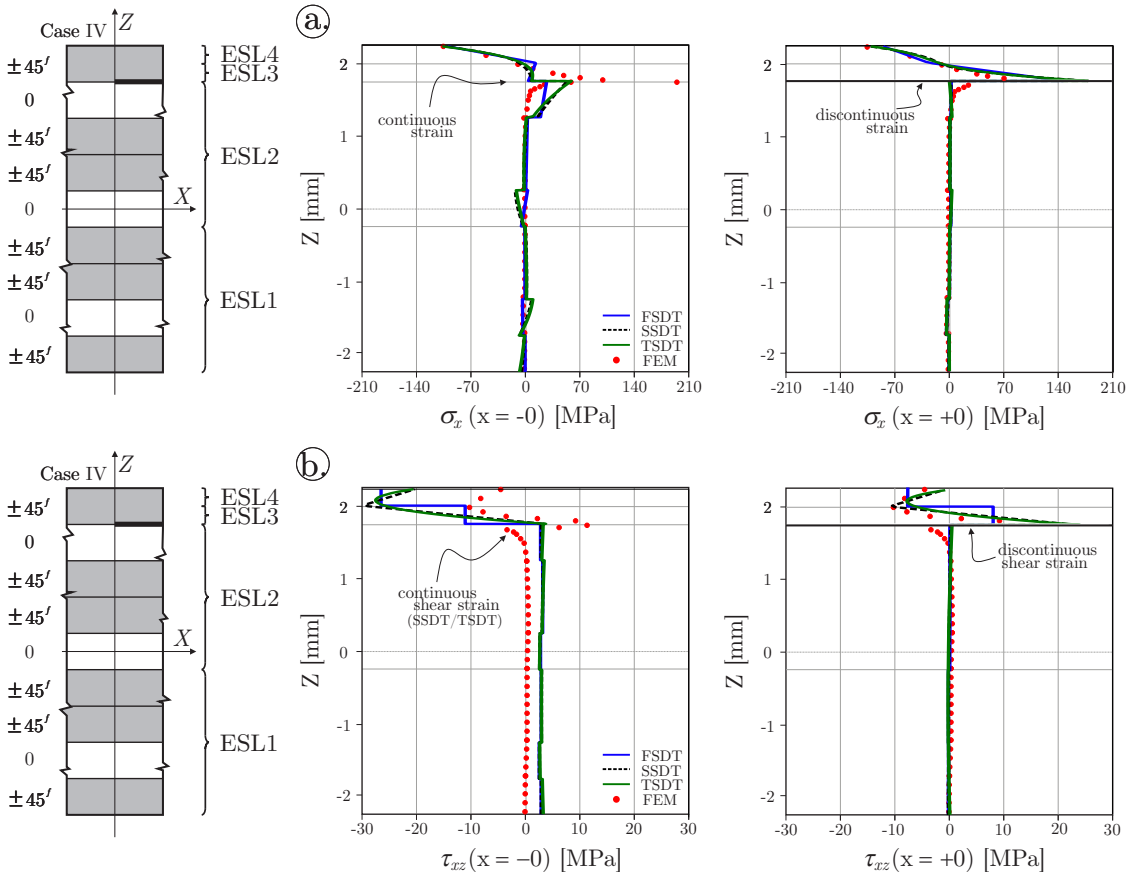

FIGURE 4.12: Distribution of the σ_x normal stresses (a) and the τ_{xz} shear stresses at the delamination tip, "Case IV", $F_t = 2$ N and $F_b =$ -2 N.

in-plane displacement compared to the "Case I" scenario we can see more changes, as well. Nevertheless, as these figures represent, there is quite good agreement between the analytical and numerical solutions. Application of SSDT and TSDT theories are not necessarily required, if the displacement terms are considered only. Although, similarly to the previous example, if stresses represent important role of the investigation the application of the

higher-order theories is inevitable and essential.

Figures 4.9 and 4.10 depict further results for "Case III" with $F_t = 10$ N and $F_b = -10$ N loadings at the end of the sub-laminates. The previously discussed phenomena is further increased by locating the delamination with one layer more above. It also enhances the σ_x normal and τ_{xz} shear stresses in the top sub-laminate. Although, the conclusions are similar to those which were concluded beforehand for "Case I" and "Case II" delamination scenarios. Obviously, the shear stresses are better approximated by SSDT and TSDT solutions.

Finally, for the sake of completeness, Figures 4.11 and 4.12 illustrate the example for "Case-IV" delamination scenario. Apparently, in this case, the loads were significantly smaller beacuse of the very thin top sub-laminate. In this example only $F_t = 2$ N and $F_b = -2$ N forces were applied at the end of the sub-laminates.

Chapter 5

J-integral

In this chapter the basic concepts of J-integral are introduced. From the general definition the application for 4ESLs is deduced. Furthermore, the decomposition of the calculated mechanical field parameters into symmetrical and asymmetrical components is discussed to perform mode separation of the enery release rates in a more exact way.

5.1 Basic definition

In order to analyse stress and strain concentrations in plane-problems including cracks and notches the so-called "J-integral" was applied. This integral has enjoyed great success as a fracture characterizing parameter because of its advantageous properties, such as path independence and its possible application for nonlinear-elastic and even elastic-plastic problems [2]. In this thesis, considering only linear elastic fracture mechanics, the most important property of this integral is the following:

$$J = G_T, \tag{5.1}$$

where G_T denotes the previously defined total energy release rate by Eq.(1.1) and J represents the value of the J-integral. Considering an abitrary counterclokwise C contour around

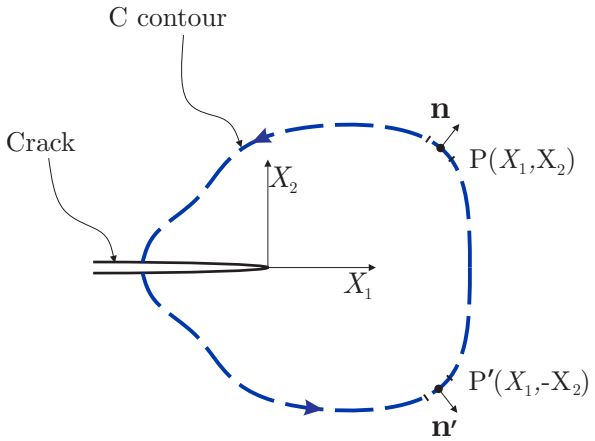

FIGURE 5.1: The general definition of the J-integral for in-plane problem.

the tip of a crack, as it is shown by Figure 5.1, the J-integral is given by:

$$\begin{aligned} J &= \int_C \left\{ U_0 n_1 - \sigma_{ij} n_j \frac{\partial u_i}{\partial x_1} \right\} ds \\ &= \int_C \left\{ \frac{1}{2} \begin{pmatrix} \sigma_{11} & \sigma_{22} & \tau_{12} \end{pmatrix} \begin{pmatrix} \varepsilon_{11} \\ \varepsilon_{22} \\ \gamma_{12} \end{pmatrix} n_1 - \begin{pmatrix} \sigma_{11} & \sigma_{22} & \tau_{12} \end{pmatrix} \begin{bmatrix} n_1 & 0 \\ 0 & n_2 \\ n_2 & n_1 \end{bmatrix} \begin{pmatrix} \partial u_1/\partial x_1 \\ \partial u_2/\partial x_1 \end{pmatrix} \right\} ds, \end{aligned} \tag{5.2}$$

where U_0 is the strain energy density, σ_{ij} and ε_{ij} are the components of the stress and strain tensors, u_i represents the displacement vector components, ds is the length increment along the C contour and n_i means the unit vector components of the outward normal vector in a given $(X_1 - X_2)$ Cartesian coordinate system [4]. In the case of delaminated beams, using semi-layerwise beam model or even classical Euler-Bernoulli model, the J-integral is calculated by applying a zero-area path integral according to the Figure 5.2a. As the J-integral is path independent this gives absolutely the same results as any other appropriate contour would give [5, 7, 8]. The strain energy density for shear deformable beam, using the Eq.(2.14) constitutive equation, can be expressed as:

$$U_0 = \frac{1}{2} \int_0^{\varepsilon_{ij}} \sigma_{ij} d\varepsilon_{ij} = \frac{1}{2} (\sigma_x \varepsilon_x + \tau_{xz} \gamma_{xz}). \tag{5.3}$$

As it is illustrated by Figure 5.2a, using the semi-layerwise beam model, $X_1 = -X$ and $X_2 = z^{(i)}$. Moreover, because of the zero-area path, the $\boldsymbol{n}$ vector is always parallel to the X axis. Taking into account the actual coordinate system and the assumed displacement field

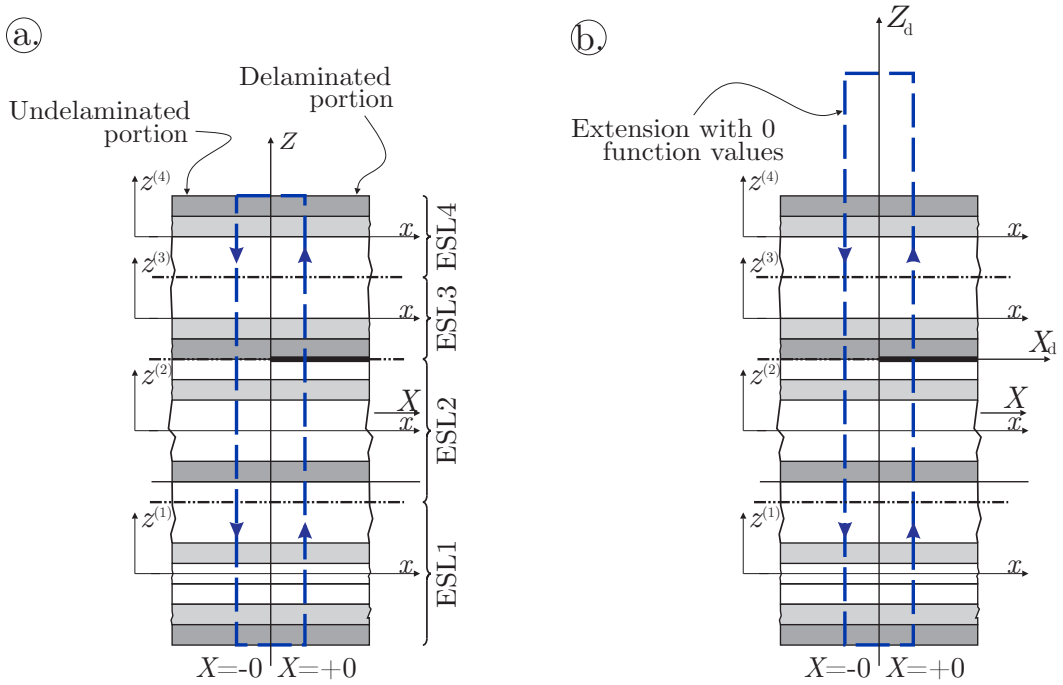

FIGURE 5.2: The application of the J-integral for semi-layerwise model using zero-area path(a) with the inevitable extension (b).

by Eq.(2.1), the G_T energy release rate can be expressed as:

$$G_T = \sum_{i=1}^{4} \int_{-t_{(i)}/2}^{t_{(i)}/2} \left\{ \left(-\frac{1}{2}\sigma_{x(i)}\varepsilon_{x(i)} + \tau_{xz(i)}\left(\frac{1}{2}\gamma_{xz(i)} - \frac{\partial w_{(i)}}{\partial x}\right)\right)\Bigg|_{x=-0}^{(undel)} + \left(\frac{1}{2}\sigma_{x(i)}\varepsilon_{x(i)} - \tau_{xz(i)}\left(\frac{1}{2}\gamma_{xz(i)} - \frac{\partial w_{(i)}}{\partial x}\right)\right)\Bigg|_{x=+0}^{(del)} \right\} dz^{(i)}, \tag{5.4}$$

where the $(undel)$ and (del) superscripts refer to the undelaminated and delaminated portion, respectively [5].

5.2 In-plane mode partitioning of the total J-integral

In order to deal in-plane fracture modes, the J-integral can be split into mode-I and mode-II parts. Although, in this case, the path of the J-integral has to be arranged reflection-symetrically to the delamination front. It was not highlighted previously because the basic defintion of the J-integral to calculate the G_T total energy release rate does not depend on it. Nevertheless, in mode partitioning, it represents a key role [2, 4]. By separating the $\varepsilon_{x(i)}$, $\gamma_{xz(i)}$ strain and $\sigma_{x(i)}$, $\tau_{xz(i)}$ stress field quantities into symmetrical and asymmetrical components with respect to the delamination plane, the mode partitioning becomes feasible. Although, apart form that case when the delamination is located exactly in the global reference plane, the position of the delamination is asymmetric. In order to make the separtion possible, first, each and every field quantity has to be shifted into the (X_d - Z_d) coordinate system. It involves only linear function transformations in terms of the ESL thicknesses. After that, the shifted field quantities within the domain $\in [-t_b, t_t]$ have to be extended through the original thickness of the beam. Because this domain does not contain any material, the values above or below the beam can be assumed to be zero value functions. This inevitable extension is shown by Figure 5.2c. Thus, the integration has to be carried out with $-t$ lower and t upper limits, where $t := max\{t_{top}, t_{bot}\}$. The symmetrical components of the strain field can be written as:

$$\begin{aligned} \varepsilon_{x(sym)} &= \frac{\varepsilon_x(-z_d) + \varepsilon_x(+z_d)}{2}, \\ \gamma_{xz(sym)} &= \frac{\gamma_{xz}(-z_d) + \gamma_{xz}(+z_d)}{2}, \end{aligned} \tag{5.5}$$

and the asymmetrical components of the strain field can obtained as:

$$\begin{aligned} \varepsilon_{x(ant)} &= \frac{\varepsilon_x(-z_d) - \varepsilon_x(+z_d)}{2} \\ \gamma_{xz(ant)} &= \frac{\gamma_{xz}(-z_d) - \gamma_{xz}(+z_d)}{2}. \end{aligned} \tag{5.6}$$

And finally the stress quantities become:

$$\begin{aligned} \sigma_{x(sym)} &= \frac{\sigma_x(-z_d) + \sigma_x(+z_d)}{2}, \\ \tau_{xz(sym)} &= \frac{\tau_{xz}(-z_d) + \tau_{xz}(+z_d)}{2}, \end{aligned} \tag{5.7}$$

and:

$$\begin{aligned} \sigma_{x(ant)} &= \frac{\sigma_x(-z_d) - \sigma_x(+z_d)}{2}, \\ \tau_{xz(ant)} &= \frac{\tau_{xz}(-z_d) - \tau_{xz}(+z_d)}{2}, \end{aligned} \tag{5.8}$$

where the (sym) and (ant) subscripts refer to the symmetrical and asymmetrical function components, respectively.

In order to make it understandable Figures 5.3 and 5.4 represent examples using previously obtained stress results (namely TSDT solution of "Case I" and "Case II"). As it was mentioned, the σ_x normal stress field function has to be shifted in to the delamination coordinate system and has to be extended with zero value function above the beam to make the

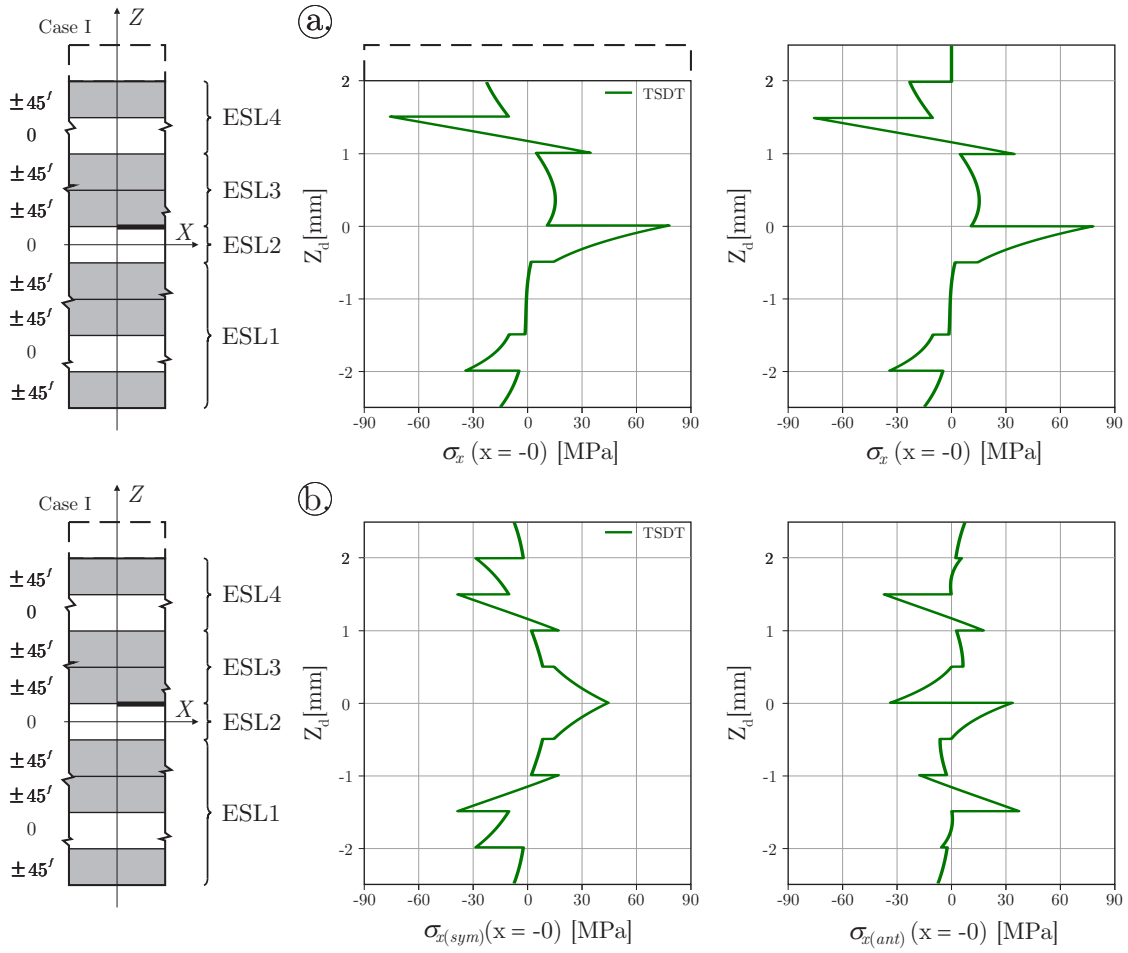

FIGURE 5.3: Tranformation of the σ_x function (a) and the obtained symmetrical and asymmetrical components of the field after the decomposition (b) for "Case-I".

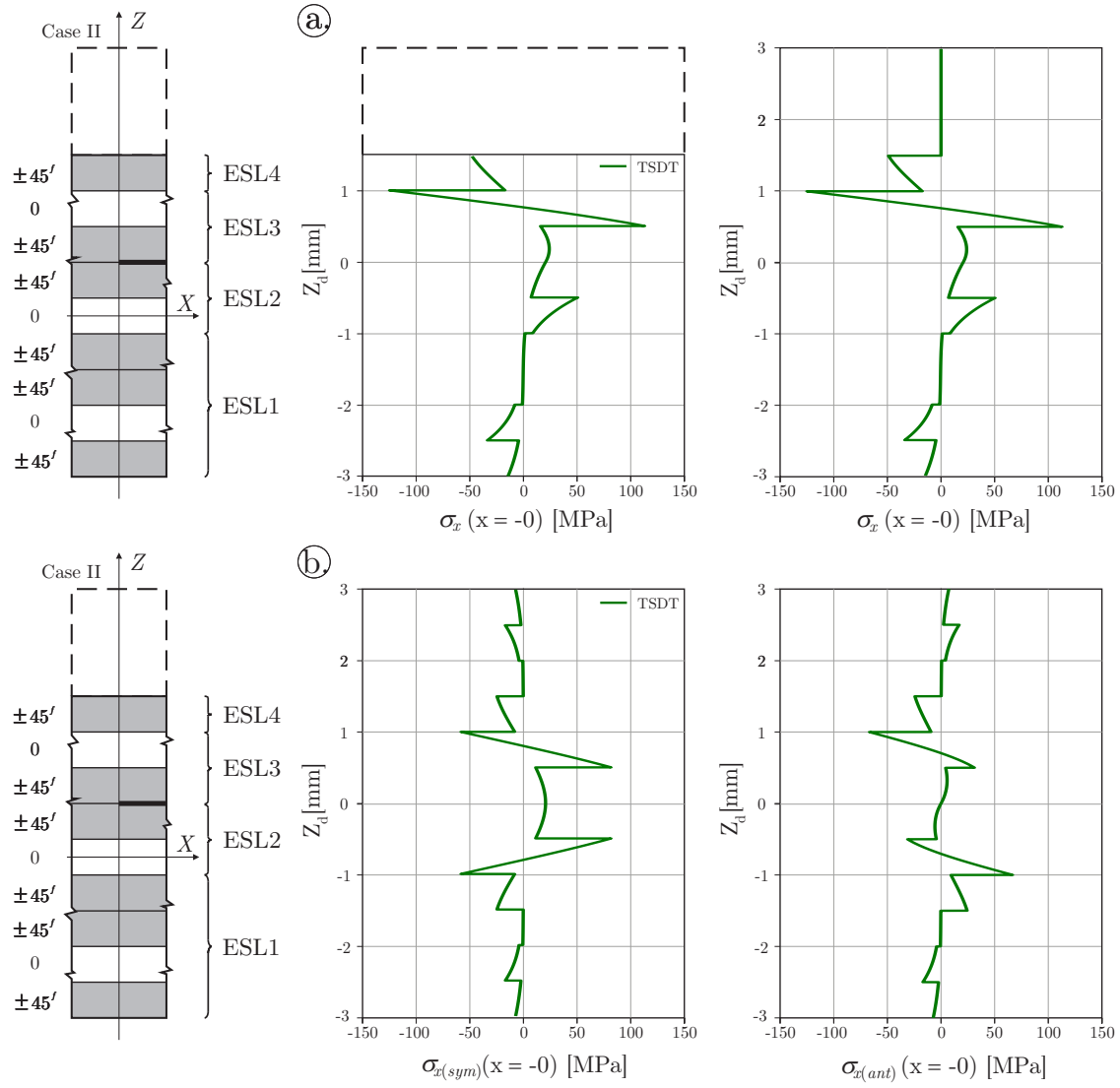

FIGURE 5.4: Tranformation of the σ_x function (a) and the obtained symmetrical and asymmetrical components of the field after the decomposition (b) for "Case-II".

domain symmetric. Thus, the decomposition beacomes performable. The obtained functions are illustrated by Figure 5.3b for "Case-I" and by Figure 5.4b for "Case-II". For the sake of completeness Figures 5.5 and 5.6 illustrate also examples for decomposition in terms of τ_{xz} shear stress using TSDT theory.

In the case of tranverse deflections, since they are independent of the Z or Z_d coordinates (referring to Eq.(3.6) and (3.18)), the decomposition can be written as:

$$\left.\frac{\partial w_{(sym)}}{\partial x}\right|_{x=-0}^{(undel)} = \left.\left(\frac{\partial w}{\partial x}\right)\right|_{x=-0}^{(undel)}, \qquad \left.\frac{\partial w_{(ant)}}{\partial x}\right|_{x=-0}^{(undel)} = 0. \tag{5.9}$$

and for the delaminated portion:

$$\left.\frac{\partial w_{(sym)}}{\partial x}\right|_{x=+0}^{(del)} = \frac{1}{2}\left.\left(\frac{\partial w_b}{\partial x} + \frac{\partial w_t}{\partial x}\right)\right|_{x=+0}^{(del)}, \qquad \left.\frac{\partial w_{(ant)}}{\partial x}\right|_{x=+0}^{(del)} = \frac{1}{2}\left.\left(\frac{\partial w_b}{\partial x} - \frac{\partial w_t}{\partial x}\right)\right|_{x=+0}^{(del)}, \tag{5.10}$$

Using these results the mode separation can be carried out as:

$$G_I = \int_{-t}^{+t} \Bigg\{ \left(-\frac{1}{2}\sigma_{x(sym)}\varepsilon_{x(sym)} + \tau_{xz(ant)}\left(\frac{1}{2}\gamma_{xz(ant)} - \frac{\partial w_{(ant)}}{\partial x}\right)\right)\Bigg|_{x=-0}^{(undel)} + \left(\frac{1}{2}\sigma_{x(sym)}\varepsilon_{x(sym)} - \tau_{xz(ant)}\left(\frac{1}{2}\gamma_{xz(ant)} - \frac{\partial w_{(ant)}}{\partial x}\right)\right)\Bigg|_{x=+0}^{(del)} \Bigg\} dz_d, \tag{5.11}$$

and:

$$G_{II} = \int_{-t}^{+t} \Bigg\{ \left(-\frac{1}{2}\sigma_{x(ant)}\varepsilon_{x(ant)} + \tau_{xz(sym)}\left(\frac{1}{2}\gamma_{xz(sym)} - \frac{\partial w_{(sym)}}{\partial x}\right)\right)\Bigg|_{x=-0}^{(undel)} + \left(\frac{1}{2}\sigma_{x(ant)}\varepsilon_{x(ant)} - \tau_{xz(sym)}\left(\frac{1}{2}\gamma_{xz(sym)} - \frac{\partial w_{(sym)}}{\partial x}\right)\right)\Bigg|_{x=+0}^{(del)} \Bigg\} dz_d. \tag{5.12}$$

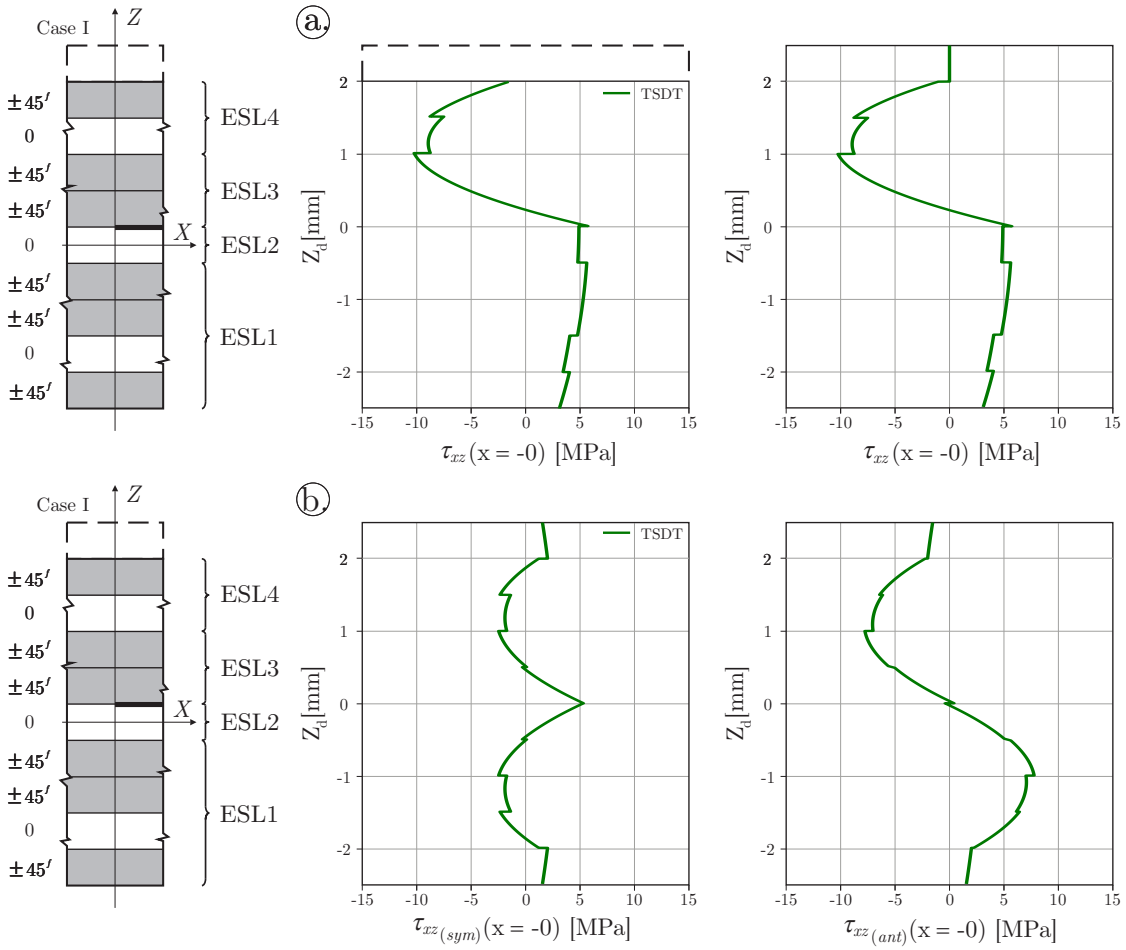

FIGURE 5.5: Tranformation of the τ_{xz} function (a) and the obtained symmetrical and asymmetrical components of the field after the decomposition (b) for "Case-I".

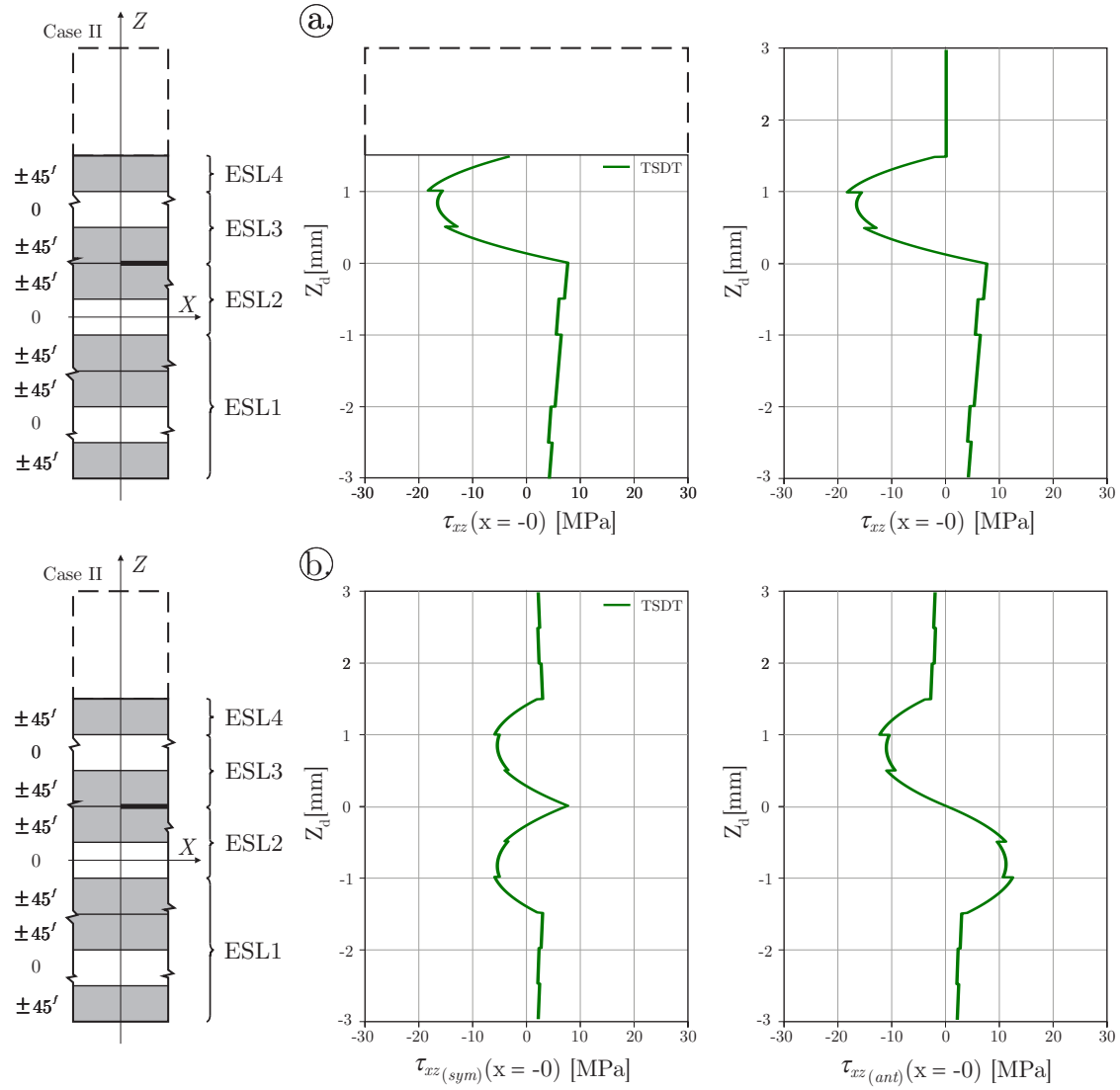

FIGURE 5.6: Tranformation of the τ_{xz} function (a) and the obtained symmetrical and asymmetrical components of the field after the decomposition (b) for "Case-II".

Using zero function extension of the field quantities above or below the delaminated beam, according to the actual location of the delamination front through the thickness, the original value of the J-integral does not change. It is also crucial from the point of mode mixity. Thus, the following relationship can always be ensured:

$$G_T = G_I + G_{II}. \tag{5.13}$$

5.3 Energy release rates and mode mixity

In this section the effects of different loading scenarios and delamination locations on the mode mixity for composite specimens are investigated and compared to FE solution. In order to help the comparison each figure shows the literature solutions, as well. These models, as it was previously discussed, are mostly based on Euler-Bernoulli theory.

The results for "Case I" and "Case II" can be seen in Figures 5.7 and 5.8. As it is depicted for each case, the higher-order theories and the Luo-Tong solution give results of mode mixity between the Williams' curvature based solution and the Bruno-Greco solution. For "Case I", when the ratio of the forces is $F_t/F_b = 1$, the higher-order theories and the Luo-Tong solution are quite close to the VCCT technique. Although, when the ratio is different from $F_t/F_b = 1$ loading case, the Luo-Tong theory predicts always the closest results to the FE solution. On the contrary, for "Case II" the SSDT theory agrees quite well with the VCCT technique and it is independent of the actual loading scenario. It is always the closest one to the FE solution.

Figures 5.9 and 5.10 depict the results for "Case III" and for "Case IV". In general, we can state that, the results of mode mixity become straighter and straighter for each theory and evaluation technique in terms of loading. Because of the very thin top sub-laminate the results are almost independent of the loading cases. It is true especially for "Case IV" where the top sub-laminate is only one thin ply. For "Case III", as it is illustrated by Figure 5.9, the higher-order theories and the Bruno-Greco solution intersect each other. The point of intersection for each case depends on the applied higher-order theory. Moreover, the Luo-Tong solution also intersects the FSDT theory. The closest solutions to the VCCT technique is the Luo-Tong solution. On the contrary, for "Case IV", the Williams' curvature solution

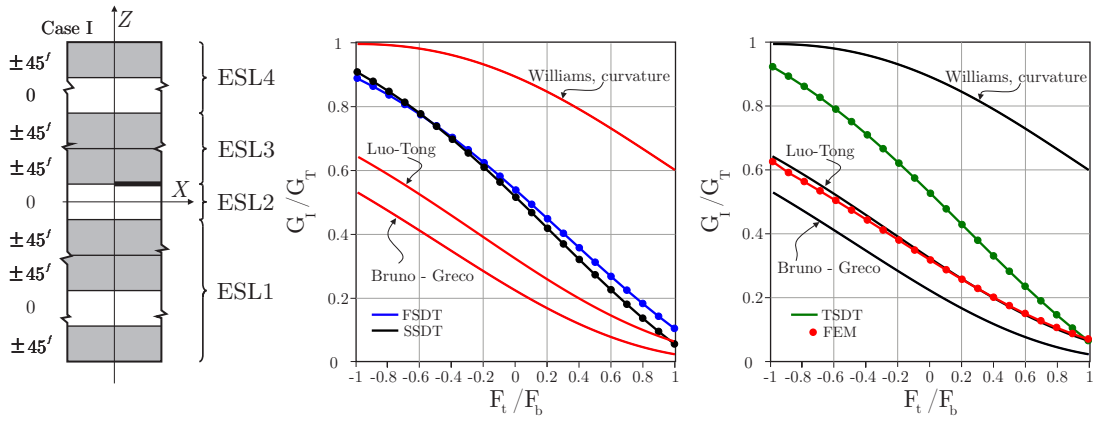

FIGURE 5.7: Mode mixity of different loading scenarios with different evaluation techniques. The delamination is located between 0 - $\pm 45^f$ layers, $a/l = 1/3$, $b = 20$ mm, $2h = 4.5$ mm.

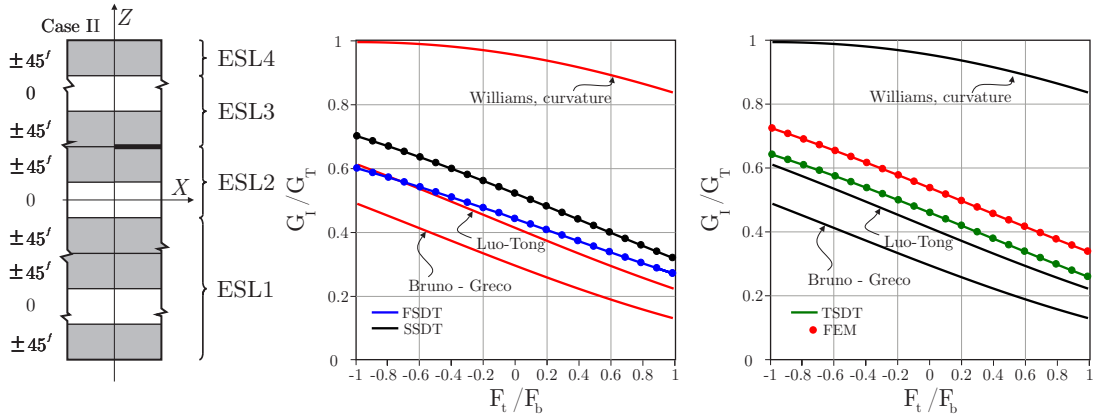

FIGURE 5.8: Mode mixity of different loading scenarios with different evaluation techniques. The delamination is located between $\pm 45^f$ - $\pm 45^f$ layers, $a/l = 1/3$, $b = 20$ mm, $2h = 4.5$ mm.

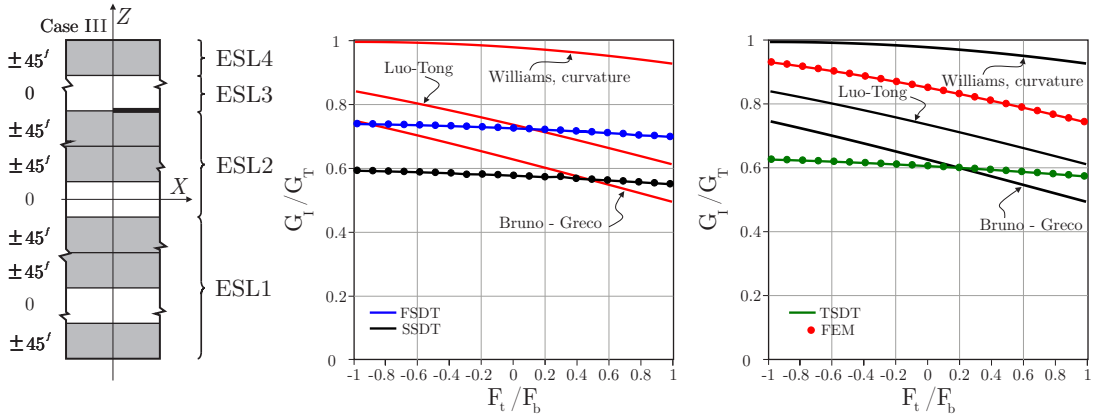

FIGURE 5.9: Mode mixity of different loading scenarios with different evaluation techniques. The delamination is located between $\pm 45^f$ - 0 layers, $a/l = 1/3$, $b = 20$ mm, $2h = 4.5$ mm.

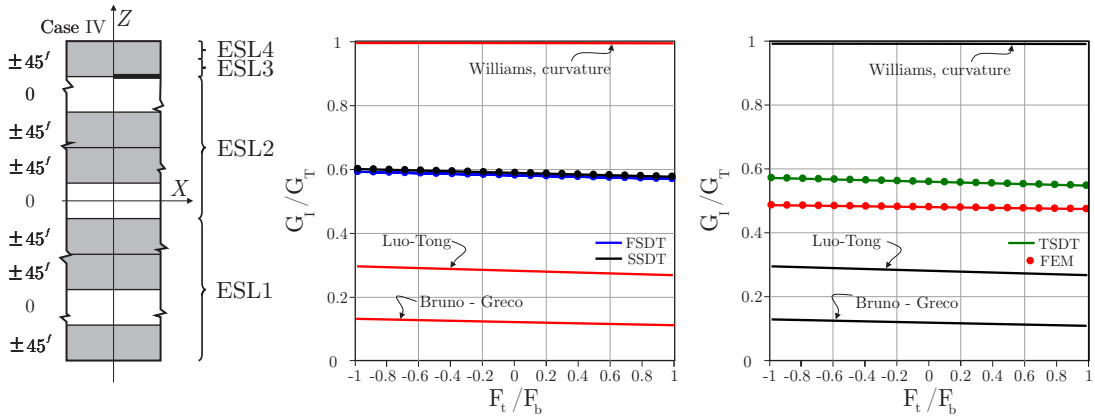

FIGURE 5.10: Mode mixity of different loading scenarios with different evaluation techniques. The delamination is located between 0 - $\pm 45^f$ layers, $a/l = 1/3$, $b = 20$ mm, $2h = 4.5$ mm.

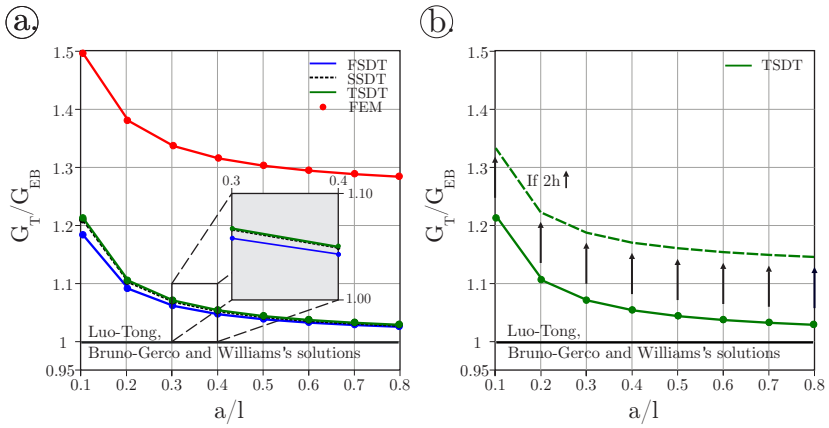

FIGURE 5.11: The ratio of the G_T total and G_{EB} energy release rates for "Case I", $F_t/F_b = -1$ (a). The effect of the $2h$ total thickness in terms of the ratio (b).

represents the worst solution from this point of view. It overpredicts significantly the results compared to the VCCT technique. For this delamination scenario the higher-order theories are the closest results to the FE solution.

In order ot get picture about the magnitude of G_T total energy release rate Figure 5.11 illustrates an example using "Case-I" configuration. Here the effect of a/l ratio on G_T is investigated with fixed $F_t/F_b = -1$ loading case. The results are normalized by the classical Euler-Bernoulli theory. Thus, we can see that the higher-order solutions, similarly to the numerical set of data, predict higher energy release rates than the classical methods if the a length of delamination decreases compared to the l total length of the beam. (Note: G_{EB} is calculated by Euler-Bernoulli beam theory.) The result can be explained by the effect of shear force. The higher-order theories are already able to take into account the strain energy which comes from the shear deformation. As the other solutions in the literature deal only with the energy which comes from the bending, they are not able to count this effect. This phenomena have been discussed in a more detailed form in my student scientific report [13]. In that report tranversely isotropic and bi-material delaminated beams were investigated and in terms of the before mentioned phenomenon the following was concluded: by increasing the $2h$ total thickness of the beam the importance of this effect becomes higher and higher. The possible magnitude tendency of G_T total energy release rate is also depicted by Figure 5.11b using TSDT theory as an example.

As a conlusion, we can state, the solutions of different methods are significantly separated from each other and predict quite different mode mixity in terms of loading cases and configurations. Actually, it is important to highlight, there is no selected solution for composite materials in the literature which could be considered as the best or the most accurate technique. From this point of view, it is absolutely an open question meaning a pioneering research topic. Nevertheless, by the application of higher-order theories and J-integral, the results of this final thesis can be considered as more exact solutions compared to the other techniques.

Summary

In this final thesis interlaminar fracture in composite beams, which can be considered as one of the most distinctive and typical form of composite damages, was investigated by using basic concepts of linear elastic fracture mechanics. Based on the virtual work principle novel semi-layerwise beam models were developed assuming the displacement field in the form of first-, second- and third-order polynomials. The kinematic continuity of the displacement fields between the contiguous ESLs was specified by using the sytem of exact kinematic conditions. The deflections were assumed with only one term in each portion. During the examples the undelaminated portion was modelled using four equivalent single layers. To describe the top and bottom sub-laminates on the delaminated portion two-two equivalent single layers were applied. The kinematic continuity conditions were imposed to the undelaminated and delaminated portions of the beam, as well. The portions were connected to each other at delamination front by expressing continuity of the displacement fields and continuity between the eqivalent stress resultants. This model was applied for built-in configuration and the displacement and stress fields were obtained at the delamination front in order to capture the complex fracture mechanical behaviour of the mechanical system.

After solving the developed system of ODEs with the necessary number of continuity and boundary conditions the *J*-integral was applied to perform in-plane fracture mechanical investigation. The obtained total energy release rate, which is the basic property of the linear elastic fracture mechanics, was separated into mode-I and mode-II components. By using symmetric and asymmetric decomposition of the strain, stress and displacement fields it became possible resulting novel and more exact mode-I/II partitioning compared to the actual solutions in the literature.

Moreover, the most important aim of this study was to investigate the mode mixity of different delamination and loading scenarios for composite beams. The effect of the delamination position through the thickness direction of the beam width with orthotropic material layers were examined based on the newly developed semi-layerwise beam models. Finally, in terms of the energy release rates, the presented solutions of the evaluation techniques were compared to previously published models in the literature of linear elastic fracture mechanics.

Összefoglalás

Diplomatervemben rétegközi törést tartalmazó kompozit rudak lineáris törésmechanikai leírására alkalmas mechanikai modellek fejlesztésével foglalkoztam. Ezen tönkremeneteli forma a szálerősített, hőre keményedő mátrixú kompozit anyagok egyik legtipikusabb és legsajátságosabb tönkremeneteli formája. A virtuális munka elvének felhasználásával, valamint az elmozdulásmezők első-, másod- és harmadrendű polinomok alakjában való közelítésével új típusú úgynevezett "szemi-réteg" modell került kifejlesztésre. A szomszédos kompozit rétegek közötti kapcsolatot az úgynevezett egzakt kinematikai peremfeltétel rendszer segítségével biztosítva, a nem delaminált rész leírására négy egyenértékű réteg, míg a delaminált részek leírására két-két egyenértékű réteget alkalmaztam. A repedéscsúcs keresztmetszetében a két modellt összeillesztettem, ezáltal előírva az elmozdulásmezők valamint az egyenértékű igénybevételek folytonosságát. A modell befogott tartón keresztül számszerűsítettem és mutattam be, ábrázolva a repedés csúcsban megjelenő alakváltozási és feszültség komponenseket. Ezáltal pontosabb és összetettebb képet kaptam a rétegközi törést tartalmazó tartó törésmechanikai viselkedéséről.

Előírva a szükséges számú folytonossági és peremfeltételeket a kapott differenciál egyenlet rendszert megoldottam. Ezt követően, a J-integrál alkalmazásával, a lineárisan rugalmas törésmechanika alapvető mennyiségét, a repedésfeszítő erőt vagy más néven energia felszabadulási rátát számítottam ki. A J-integrál alkalmazásával továbbá lehetőség nyílt annak I-es és II-es módusokra való szétválasztására, amely így, az eddigi módszerekhez képest, jóval egzaktabb megoldásnak tekinthető. Ehhez a repedéscsúcsban lévő elmozdulásokat, fajlagos alakváltozásokat és feszültségeket kellett szétbontani a repedésfrontra szimmetrikus és aszimmetrikus függvényekre.

Dolgozatom legvégén, az egyes törésmechanikai módusok arányát a delamináció helyzetének és befogott kompozit rúd terhelésének függvényében vizsgáltam. A kapott módus arányokat numerikus eredményekkel, valamint a szakirodalomban elérhető referencia megoldásokkal hasonlítottam össze.

Bibliography

[1] J.N.Reddy: Mechanics of Laminated Composite Plates and Shells - Theory and Analysis, Second edition, *Boca Raton, London, New York, Washington D.C.*, CRC Press, 2004.

[2] T.L.Anderson: Fracture Mechanincs - Fundamentals and Applications, Third Edition, *Boca Raton, London, New York, Washington D.C.*, 2005.

[3] Stephen W. Tsai: Theory of composite design, *Stranford University*, 2008.

[4] Meinhard Kuna: Finite elements in Fracture Mechanics Theory-Numerics-Applications, Springer, *Dordrecht Heidelberg New York London*, 2010.

[5] A.Szekrényes: Nonsingular delamination modeling in orthotropic composit plates by semi-layerwise analysis, DSc dissertation, *Budapest, Budapest University of Technology and Economics, Department of Applied Mechanics*, 2016.

[6] A.Szekrényes: Delamination of composite specimens, Ph. D. dissertation, *Budapest, Budapest University of Technology and Economics, Department of Applied Mechanics*, 2005.

[7] A.Szekrényes: Nonsingular crack modelling in orthotropic plates by four equivalent single layers, *Europen Journal of Mechanics A/Solids 55 73-99*, 2016.

[8] A.Szekrényes: Semi-layerwise analysis of laminated plates with nonsingular delamination - The theorem of autocontinuity, *Applied Mathematical Modelling 40, 1344–1371*, 2016.

[9] J.G.Williams : On the calculation of energy release rates for cracked laminates, *Internation Journal of Fracture 36 2 101-119*, 1988.

[10] Domenico Bruno, Fabrizio Greco: Mixed mode delamination in plates: a refined approach, *Internation Journal of Solids and Structures 38 50-51 9149-9177*, 2001.

[11] Quantian Luo, Liyong Tong: Analytic formulas of energy release rates for delamination using a global–local method, *Internation Journal of Solids and Structures 49 23-24 3335-3344* , 2012.

[12] A.Leski: Implementation of the virtual crack closure technique in engineering FE calculations, *Finite Elements in Analysis and Design 43 261-268*, 2006.

[13] B. Kiss: Evaluation of fracture mechanical tests on composite beams by the J-integral and higher-order theories - Student Scientific Report, *Budapest University of Technology and Economics, Department of Applied Mechanics*, 2018.

[14] G. Czél: Composite technology - Lecture notes, *Budapest University of Technology and Economics, Department of Polymer Engineering*, 2018.

Appendix A

Matrix elements - Method of 4ESLs

A.1 Third-order beam theory

This Appendix collects the K_{ij} matrix elements for the third-order beam theory.

Undelaminated region

$$K_{11}^{(0)} = -z_R^{(2)} - \frac{t_1+t_2}{2}, \tag{A.1}$$

$$K_{12}^{(0)} = \frac{(t_1+t_2+z_R^{(2)})(t_1^2+2t_1t_2-2t_1z_R^{(2)}-2t_2^2-2t_2z_R^{(2)}+4[z_R^{(2)}]^2)}{12(t_1+t_2)}, \tag{A.2}$$

$$K_{13}^{(0)} = \frac{(t_1+t_2+z_R^{(2)})(2t_1^2+10t_1t_2-4t_1z_R^{(2)}+11t_2^2-4t_2z_R^{(2)}-4[z_R^{(2)}]^2)}{12(t_1+t_2)}, \tag{A.3}$$

$$K_{14}^{(0)} = \frac{(3t_3+2t_4)(t_1+t_2+2z_R^{(2)})t_3}{4(t_3+t_4)},\ K_{15}^{(0)} = -\frac{(t_1+t_2+2z_R^{(2)})t_3}{4(t_3+t_4)}, \tag{A.4}$$

$$K_{21}^{(0)} = -z_R^{(2)},\ K_{22}^{(0)} = -\frac{(3t_2^2-4[z_R^{(2)}]^2)z_R^{(2)}}{6(t_1+t_2)}, \tag{A.5}$$

$$K_{23}^{(0)} = \frac{(6t_1t_2-6t_1z_R^{(2)}+9t_2^2-6t_2z_R^{(2)}-4[z_R^{(2)}]^2)}{6(t_1+t_2)},\ K_{24}^{(0)} = \frac{(3t_3+2t_4)t_3z_R^{(2)}}{2(t_3+t_4)}, \tag{A.6}$$

$$K_{25}^{(0)} = -\frac{t_3^2z_R^{(2)}}{2(t_3+t_4)},\ K_{31}^{(0)} = \frac{t_2+t_3}{2} - z_R^{(2)},\ K_{32}^{(0)} = \frac{(t_2+z_R^{(2)})(t_2-2z_R^{(2)})^2}{t_1+t_2}, \tag{A.7}$$

$$K_{33}^{(0)} = -\frac{(t_2-2z_R^{(2)})^2(3t_1+5t_2+2z_R^{(2)})}{12(t_1+t_2)}, \tag{A.8}$$

$$K_{34}^{(0)} = -\frac{(9t_2t_3 + 6t_2t_4 + 4t_3^2 + 3t_3t_4 - 18t_3z_R^{(2)} - 12t_4z_R^{(2)})t_3}{12(t_3+t_4)}, \tag{A.9}$$

$$K_{35}^{(0)} = \frac{(3t_2 + t_3 - 6z_R^{(2)})t_3^2}{12(t_3+t_4)},\ K_{41}^{(0)} = \frac{t_2+t_4}{2} + t_3 - z_R^{(2)}, \tag{A.10}$$

$$K_{42}^{(0)} = \frac{(t_2 + z_R^{(2)})(t_2 - 2z_R^{(2)})^2}{t_1+t_2},\ K_{43}^{(0)} = -\frac{(t_2 - 2z_R^{(2)})^2(3t_1 + 5t_2 + 2z_R^{(2)})}{12(t_1+t_2)}, \tag{A.11}$$

$$K_{44}^{(0)} = -\frac{9t_2t_3^2 + 6t_2t_3t_4 + 2t_3^2 - 3t_3^2t_4 - 18t_3^2z_R^{(2)} - 6t_3t_4^2 - 12t_3t_4z_R^{(2)} - 2t_4^3}{12(t_3+t_4)}, \tag{A.12}$$

$$K_{44}^{(0)} = \frac{3t_2t_3^2 + 2t_3^3 + 3t_3^2t_4 - 6t_3^2z_R^{(2)} + 3t_3t_4^2 + t_4^3}{12(t_3+t_4)}, \tag{A.13}$$

$$K_{11}^{(1)} = 1,\ K_{12}^{(1)} = -\frac{t_1(t_1+2t_2)}{2(t_1+t_2)},\ K_{13}^{(1)} = -\frac{(t_1+2t_2)}{2(t_1+t_2)^2}, \tag{A.14}$$

$$K_{14}^{(1)} = -\frac{(3t_3+2t_4)t_3}{2(t_3+t_4)},\ K_{15}^{(1)} = \frac{t_3^2}{2(t_3+t_4)},\ K_{21}^{(1)} = 1,\ K_{22}^{(1)} = \frac{t_2^2}{2(t_1+t_2)}, \tag{A.15}$$

$$K_{23}^{(1)} = -\frac{(2t_1+3t_2)t_2}{2(t_1+t_2)},\ K_{24}^{(1)} = -\frac{(3t_3+2t_4)t_3}{2(t_3+t_4)},\ K_{25}^{(1)} = \frac{t_3^2}{2(t_3+t_4)}, \tag{A.16}$$

$$K_{31}^{(1)} = 1,\ K_{32}^{(1)} = K_{33}^{(1)} = K_{34}^{(1)} = K_{35}^{(1)} = 0,\ K_{41}^{(1)} = 1,\ K_{42}^{(1)} = K_{43}^{(1)} = 0, \tag{A.17}$$

$$K_{44}^{(1)} = \frac{t_3+t_4}{2},\ K_{45}^{(1)} = \frac{t_3+t_4}{2}, \tag{A.18}$$

$$K_{11}^{(2)} = 0,\ K_{12}^{(2)} = 1,\ K_{13}^{(2)} = K_{14}^{(2)} = K_{15}^{(2)} = K_{21}^{(2)} = K_{22}^{(2)} = 0,\ K_{23}^{(2)} = 1, \tag{A.19}$$

$$K_{24}^{(2)} = K_{25}^{(2)} = K_{31}^{(2)} = K_{32}^{(2)} = K_{33}^{(2)} = 0,\ K_{34}^{(2)} = 1, \tag{A.20}$$

$$K_{35}^{(2)} = K_{41}^{(2)} = K_{42}^{(2)} = K_{43}^{(2)} = K_{44}^{(2)}, \; K_{45}^{(2)} = 1, \tag{A.21}$$

$$K_{11}^{(3)} = 0, \; K_{12}^{(3)} = -\frac{2}{3(t_1+t_2)}, \; K_{13}^{(3)} = \frac{2}{3(t_1+t_2)}, \; K_{14}^{(3)} = K_{15}^{(3)} = K_{21}^{(3)} = 0, \tag{A.22}$$

$$K_{22}^{(3)} = -\frac{2}{3(t_1+t_2)}, \; K_{23}^{(3)} = \frac{2}{3(t_1+t_2)}, \tag{A.23}$$

$$K_{24}^{(3)} = K_{25}^{(3)} = K_{31}^{(3)} = K_{32}^{(3)} = K_{33}^{(3)} = 0, \; K_{34}^{(3)} = -\frac{2}{3(t_3+t_4)}, \tag{A.24}$$

$$K_{35}^{(3)} = \frac{2}{3(t_3+t_4)}, \; K_{41}^{(3)} = K_{42}^{(3)} = K_{43}^{(3)} = 0, \tag{A.25}$$

$$K_{44}^{(3)} = -\frac{2}{3(t_3+t_4)}, \; K_{45}^{(3)} = \frac{2}{3(t_3+t_4)}. \tag{A.26}$$

Delaminated region

$$K_{11}^{(0)} = -\frac{t_2}{2}, \; K_{12}^{(0)} = -\frac{t_2^3(3t_1+2t_2)}{12(t_1+t_2)}, \; K_{13}^{(0)} = -\frac{t_2^3}{12(t_1+t_2)}, \tag{A.27}$$

$$K_{14}^{(0)} = K_{15}^{(0)} = K_{16}^{(0)} = 0, \; K_{21}^{(0)} = \frac{t_1}{2}, \; K_{22}^{(0)} = \frac{t_1(2t_1^2+6t_1t_2+3t_2^2)}{12(t_1+t_2)}, \tag{A.28}$$

$$K_{23}^{(0)} = \frac{t_1(2t_1^2+3t_1t_2+3t_2^2)}{12(t_1+t_2)}, \; K_{24}^{(0)} = K_{25}^{(0)} = K_{26}^{(0)} = K_{31}^{(0)} = K_{32}^{(0)} = K_{33}^{(0)} = 0, \tag{A.29}$$

$$K_{34}^{(0)} = -\frac{t_4}{2}, \; K_{35}^{(0)} = -\frac{t_4^2(3t_3+2t_4)}{12(t_3+t_4)}, \; K_{36}^{(0)} = -\frac{t_4^2}{12(t_3+t_4)}, \tag{A.30}$$

$$K_{41}^{(0)} = K_{42}^{(0)} = K_{43}^{(0)} = 0, \; K_{44}^{(0)} = \frac{t_3}{2}, \; K_{45}^{(0)} = \frac{t_3(2t_3^2+6t_1t_3+3t_4^2)}{12(t_3+t_4)}, \tag{A.31}$$

$$K_{46}^{(0)} = \frac{t_3(2t_3^2+3t_3t_4+3t_4^2)}{12(t_3+t_4)}, \tag{A.32}$$

$$K_{11}^{(1)} = 1,\ K_{12}^{(1)} = K_{13}^{(1)} = K_{14}^{(1)} = K_{15}^{(1)} = K_{16}^{(1)} = 0,\ K_{21}^{(1)} = 1,\ K_{22}^{(1)} = K_{23}^{(1)} = \frac{t1+t2}{2}, \tag{A.33}$$

$$K_{24}^{(1)} = K_{25}^{(1)} = K_{26}^{(1)} = K_{31}^{(1)} = K_{32}^{(1)} = K_{33}^{(1)} = 0,\ K_{34}^{(1)} = 1, \tag{A.34}$$

$$K_{35}^{(1)} = K_{36}^{(1)} = K_{41}^{(1)} = K_{42}^{(1)} = K_{43}^{(1)} = 0,\ K_{44}^{(1)} = 1,\ K_{45}^{(1)} = K_{46}^{(1)} = \frac{t_3+t_4}{2}, \tag{A.35}$$

$$K_{11}^{(2)} = 0,\ K_{12}^{(2)} = 1,\ K_{13}^{(2)} = K_{14}^{(2)} = K_{15}^{(2)} = K_{16}^{(2)} = K_{21}^{(2)} = K_{22}^{(2)} = 0,\ K_{23}^{(2)} = 1, \tag{A.36}$$

$$K_{24}^{(2)} = K_{25}^{(2)} = K_{26}^{(2)} = K_{31}^{(2)} = K_{32}^{(2)} = K_{33}^{(2)} = K_{34}^{(2)} = 0,\ K_{35}^{(2)} = 1, \tag{A.37}$$

$$K_{36}^{(2)} = K_{41}^{(2)} = K_{42}^{(2)} = K_{43}^{(2)} = K_{44}^{(2)} = K_{45}^{(2)} = 0,\ K_{46}^{(2)} = 1, \tag{A.38}$$

$$K_{11}^{(3)} = 0,\ K_{12}^{(3)} = -\frac{2}{3(t_1+t_2)},\ K_{13}^{(3)} = \frac{2}{3(t_1+t_2)},\ K_{14}^{(3)} = K_{15}^{(3)} = K_{16}^{(3)} = K_{21}^{(3)} = 0, \tag{A.39}$$

$$K_{22}^{(3)} = -\frac{2}{3(t_1+t_2)},\ K_{23}^{(3)} = \frac{2}{3(t_1+t_2)}, \tag{A.40}$$

$$K_{24}^{(3)} = K_{25}^{(3)} = K_{26}^{(3)} = K_{31}^{(3)} = K_{32}^{(3)} = K_{33}^{(3)} = K_{34}^{(3)} = 0,\ K_{35}^{(3)} = -\frac{2}{3(t_3+t_4)}, \tag{A.41}$$

$$K_{36}^{(3)} = \frac{2}{3(t_3+t_4)},\ K_{41}^{(3)} = K_{42}^{(3)} = K_{43}^{(3)} = K_{44}^{(3)} = 0,\ K_{45}^{(3)} = -\frac{2}{3(t_3+t_4)}, \tag{A.42}$$

$$K_{46}^{(3)} = \frac{2}{3(t_3+t_4)}. \tag{A.43}$$

A.2 Second-order beam theory

In this Appendix the K_{ij} matrix elements for the second-order beam theory are presented.

Undelaminated region

$$K_{11}^{(0)} = -z_R^{(2)} - \frac{t_1+t_2}{2},\ K_{12}^{(0)} = 0,\ K_{13}^{(0)} = -\frac{t_1}{4}(t_1+2t_2+4z_R^{(2)}), \tag{A.44}$$

$$K_{14}^{(0)} = -\frac{(t_2+2z_R^{(2)})^2}{4},\ K_{15}^{(0)} = 0,\ K_{21}^{(0)} = -z_R^{(2)},\ K_{22}^{(0)} = 0,\ K_{23}^{(0)} = -t_1 z_R^{(2)}, \tag{A.45}$$

$$K_{24}^{(0)} = -z_R^{(2)}(t_2+z_R^{(2)}),\ K_{25}^{(0)} = 0,\ K_{31}^{(0)} = \frac{t_3}{4}+\frac{t_2}{2}-z_R^{(2)},\ K_{32}^{(0)} = \frac{t_3}{4}, \tag{A.46}$$

$$K_{33}^{(0)} = \frac{t_1}{4}(t_3+2t_2-4z_R^{(2)}),\ K_{34}^{(0)} = \frac{t_2t_3}{2}+\frac{3t_2^2}{4}-t_2z_R^{(2)}-[z_R^{(2)}]^2, \tag{A.47}$$

$$K_{35}^{(0)} = 0,\ K_{41}^{(0)} = \frac{t_2-t_4}{2}-z_R^{(2)},\ K_{42}^{(0)} = t_3+t_4,\ K_{43}^{(0)} = \frac{t_1}{2}(t_2-t_4-2z_R^{(2)}), \tag{A.48}$$

$$K_{44}^{(0)} = \frac{3t_2^2}{4}-t_2t_4-t_2z_R^{(2)},\ K_{45}^{(0)} = \frac{t_4^2}{4}. \tag{A.49}$$

$$K_{11}^{(1)} = 1,\ K_{12}^{(1)} = K_{13}^{(1)} = K_{14}^{(1)} = K_{15}^{(1)} = 0,\ K_{21}^{(1)} = 1,\ K_{22}^{(1)} = 0,\ K_{23}^{(1)} = t_1, \tag{A.50}$$

$$K_{24}^{(1)} = t_2,\ K_{25}^{(1)} = K_{31}^{(1)} = K_{32}^{(1)} = K_{34}^{(1)} = K_{35}^{(1)} = 0,\ K_{41}^{(1)} = -1, \tag{A.51}$$

$$K_{42}^{(1)} = 2,\ K_{43}^{(1)} = -t_1,\ K_{44}^{(1)} = -2t_2,\ K_{45}^{(1)} = t_4,\ K_{11}^{(2)} = K_{12}^{(2)} = 0, \tag{A.52}$$

$$K_{13}^{(2)} = 1,\ K_{14}^{(2)} = K_{15}^{(2)} = K_{21}^{(2)} = K_{22}^{(2)} = K_{23}^{(2)} = 0, \tag{A.53}$$

$$K_{24}^{(2)} = 1,\ K_{25}^{(2)} = 0,\ K_{31}^{(2)} = -\frac{1}{t_3},\ K_{32}^{(2)} = \frac{1}{t_3},\ K_{33}^{(2)} = -\frac{t_1}{t_3},\ K_{34}^{(2)} = -\frac{2t_2}{t_3}, \tag{A.54}$$

$$K_{35}^{(2)} = K_{41}^{(2)} = K_{42}^{(2)} = K_{43}^{(2)} = K_{44}^{(2)} = 0,\ K_{45}^{(2)} = 1 \tag{A.55}$$

Delaminated region

$$K_{11}^{(0)} = -\frac{t_2}{2},\ K_{12}^{(0)} = -\frac{t_2^2}{4},\ K_{13}^{(0)} = K_{14}^{(0)} = K_{15}^{(0)} = K_{16}^{(0)} = 0,\ K_{21}^{(0)} = \frac{t_1}{2}, \tag{A.56}$$

$$K_{22}^{(0)} = \frac{t_1^2}{4} + \frac{t_1 t_2}{2} - \frac{t_2^2}{4},\ K_{23}^{(0)} = \frac{t_2^2}{4},\ K_{24}^{(0)} = K_{25}^{(0)} = K_{26}^{(0)} = K_{31}^{(0)} = K_{32}^{(0)} = K_{33}^{(0)} = 0, \tag{A.57}$$

$$K_{34}^{(0)} = -\frac{t_4}{2},\ K_{35}^{(0)} = -\frac{t_4^2}{4},\ K_{36}^{(0)} = K_{41}^{(0)} = K_{42}^{(0)} = K_{43}^{(0)} = 0,\ K_{44}^{(0)} = \frac{t_3}{2}, \tag{A.58}$$

$$K_{45}^{(0)} = \frac{t_3^2}{4} + \frac{t_3 t_4}{2} - \frac{t_4^2}{4},\ K_{45}^{(0)} = \frac{t_4^2}{4} \tag{A.59}$$

$$K_{11}^{(1)} = 1,\ K_{12}^{(1)} = K_{13}^{(1)} = K_{14}^{(1)} = K_{15}^{(1)} = K_{16}^{(1)},\ K_{21}^{(1)} = 1,\ K_{22}^{(1)} = t_1,\ K_{23}^{(1)} = t_2, \tag{A.60}$$

$$K_{24}^{(1)} = K_{25}^{(1)} = K_{26}^{(1)} = K_{31}^{(1)} = K_{32}^{(1)} = K_{33}^{(1)} = 0,\ K_{34}^{(1)} = 1, \tag{A.61}$$

$$K_{35}^{(1)} = K_{36}^{(1)} = K_{41}^{(1)} = K_{42}^{(1)} = K_{43}^{(1)} = 0,\ K_{44}^{(1)} = 1,\ K_{45}^{(1)} = t_3,\ K_{46}^{(1)} = t_4, \tag{A.62}$$

$$K_{11}^{(2)} = 0,\ K_{12}^{(2)} = 1,\ K_{13}^{(2)} = K_{14}^{(2)} = K_{15}^{(2)} = K_{16}^{(2)} = K_{21}^{(2)} = K_{22}^{(2)} = 0, \tag{A.63}$$

$$K_{23}^{(2)} = 1,\ K_{24}^{(2)} = K_{25}^{(2)} = K_{26}^{(2)} = K_{31}^{(2)} = K_{32}^{(2)} = K_{33}^{(2)} = K_{34}^{(2)} = 0;\ K_{35}^{(2)} = 1, \tag{A.64}$$

$$K_{36}^{(2)} = K_{41}^{(2)} = K_{42}^{(2)} = K_{43}^{(2)} = K_{44}^{(2)} = K_{45}^{(2)},\ K_{46}^{(2)} = 1. \tag{A.65}$$

A.3 First-order beam theory

This Appendix collects the K_{ij} matrix elements of the FSDT solution.

Undelaminated region

$$K_{11}^{(0)} = -\frac{t_1}{2},\ K_{12}^{(0)} = -\frac{t_2}{2} - z_R^{(2)},\ K_{13}^{(0)} = K_{14}^{(0)} = K_{21}^{(0)} = 0,\ K_{22}^{(0)} = -z_R^{(2)}, \tag{A.66}$$

$$K_{23}^{(0)} = K_{24}^{(0)} = K_{31}^{(0)} = 0,\ K_{32}^{(0)} = \frac{t_2}{2} - z_R^{(2)},\ K_{33}^{(0)} = \frac{t_3}{2},\ K_{34}^{(0)} = K_{41}^{(0)} = 0, \tag{A.67}$$

$$K_{42}^{(0)} = \frac{t_2}{2} - z_R^{(2)},\ K_{43}^{(0)} = t_3,\ K_{44}^{(0)} = \frac{t_4}{2} \tag{A.68}$$

$$K_{11}^{(1)} = 1,\ K_{12}^{(1)} = K_{13}^{(1)} = K_{14}^{(1)} = K_{21}^{(1)} = 0,\ K_{22}^{(1)} = 1,\ K_{23}^{(1)} = K_{24}^{(1)} = 0 \tag{A.69}$$

$$K_{31}^{(1)} = K_{32}^{(1)} = 0,\ K_{33}^{(1)} = 1,\ K_{34}^{(1)} = K_{41}^{(1)} = K_{42}^{(1)} = K_{43}^{(1)} = 0,\ K_{44}^{(1)} = 0. \tag{A.70}$$

Delaminated region

$$K_{11}^{(0)} = -\frac{t_2}{2},\ K_{12}^{(0)} = K_{13}^{(0)} = K_{14}^{(0)} = 0,\ K_{21}^{(0)} = \frac{t_1 - t_2}{2},\ K_{22}^{(0)} = \frac{t_2}{2}, \tag{A.71}$$

$$K_{23}^{(0)} = K_{24}^{(0)} = 0,\ K_{31}^{(0)} = K_{32}^{(0)} = 0,\ K_{33}^{(0)} = -\frac{t_4}{2}, \tag{A.72}$$

$$K_{34}^{(0)} = K_{41}^{(0)} = K_{42}^{(0)} = 0,\ K_{43}^{(0)} = \frac{t_3 - t_4}{2},\ K_{44}^{(0)} = \frac{t_4}{2}, \tag{A.73}$$

$$K_{11}^{(1)} = 1,\ K_{12}^{(1)} = K_{13}^{(0)} = K_{14}^{(0)} = 0,\ K_{21}^{(1)} = 0,\ K_{22}^{(1)}1,\ K_{23}^{(1)} = K_{24}^{(0)} = 0, \tag{A.74}$$

$$K_{31}^{(1)} = K_{32}^{(1)} = 0,\ K_{33}^{(1)} = 1,\ K_{34}^{(1)} = 0,\ K_{41}^{(1)} = K_{42}^{(1)} = K_{43}^{(1)} = 0,\ K_{44}^{(1)} = 1. \tag{A.75}$$